THE ASTROPHYSICAL JOURNAL SUPPLEMENT SERIES, 70:699–722, 1989 August

GLOBAL PROPERTIES OF INFRARED BRIGHT GALAXIES

JUDITH S. YOUNG[1,2] SHUDING XIE,[1] JEFFREY D. P. KENNEY,[1,3] AND WALTER L. RICE[4]
Received 1988 July 13; accepted 1988 November 22

ABSTRACT

We have analyzed the *IRAS* data for 182 galaxies in order to determine accurate measures of their total flux densities, especially for galaxies that are partially resolved by *IRAS*. These galaxies are a subset of a complete, magnitude-limited sample whose molecular contents are being measured using the Five College Radio Astronomy Observatory (FCRAO) 14 m millimeter telescope as part of the FCRAO Extragalactic CO Survey. Here, we present IR flux densities at 12, 25, 60, and 100 μm from co-added *IRAS* data, including results for 50 galaxies in the Virgo cluster. For galaxies with optical diameters between 5′ and 8′, we find that the Point Source Catalog (PSC) typically underestimates the flux density by a factor of 2 at 60 μm and by a factor of 1.5 at 100 μm. Furthermore, flux densities at 12 and 25 μm are reported for 63 galaxies for which only upper limits are reported in the PSC.

IR luminosities, colors, and warm dust masses are derived for the 182 galaxies, and these quantities are compared with the interstellar gas masses and optical luminosities of the galaxies. The H_2 masses reported here have been derived from models for the source distributions and are corrected for source-beam coupling for our previously published CO observations of 124 galaxies. The IR luminosity is found to correlate better with the molecular mass than with the total H I mass or the total H I + H_2 mass for galaxies with L_{IR} above 10^{10} $L_\odot$. This is consistent with the IR emission arising primarily from dust in molecular clouds for galaxies with $L_{IR} > 10^{10}$ $L_\odot$ since the interstellar medium (ISM) with the inner disk for these galaxies is primarily molecular. The best correlation we find is that between the warm dust masses inferred from *IRAS* data and the molecular masses derived from CO observations, such that $M(H_2) \propto M_{dust}^{1.0}$. The mean value of $M(H_2)/M_{dust}$ in this sample is 570 ± 50; that this value is higher than 100 probably reflects the fact that *IRAS* is not sensitive to the cold dust emitting beyond 120 μm.

From fits to the comparisons of L_{IR} and L_B with $M(H_2)$ and M(H I), we find that $L_{IR} \propto M(H_2)^{1.0}$ and $L_B \propto M(H_2)^{0.72}$, with similar exponents for the comparison of L_{IR} and L_B with M(H I). We suggest that extinction may lower the blue luminosities in the most luminous galaxies relative to the IR luminosity, since the luminous galaxies have higher H_2 surface densities and therefore larger dust column densities in their central regions.

We demonstrate that the IR luminosity is a measure of the star formation rate for this sample from the correlation of Hα and IR luminosities. If L_{IR} measures the star formation rate, then the ratio $L_{IR}/M(H_2)$ measures the stellar luminosity per unit H_2 mass, which we call the star formation efficiency. Furthermore, we find a good correlation between $L_{IR}/M(H_2)$ and the global Hα equivalent widths for 26 late-type spiral galaxies, from which we suggest that galaxies that are forming large numbers of high-mass stars are doing so through efficient conversion of gas into stars.

Subject headings: galaxies: clustering — galaxies: interstellar matter — galaxies: photometry — infrared: sources — stars: formation

I. INTRODUCTION

The availability of sensitive observations of the infrared emission of galaxies made possible by the *IRAS* satellite has infused new life into studies of the structure and evolution of galaxies. While there is general agreement that the IR emission arises from heated dust in galaxies (see Rieke *et al.* 1980; Telesco and Harper 1980; de Jong *et al.* 1984; Soifer *et al.* 1984), there are numerous suggestions for the heating sources of this dust (see Young *et al.* 1986*b*; Lonsdale and Helou 1987; Harwit *et al.* 1986; Rowan-Robinson and Crawford 1986; Becklin and Wynn-Williams 1987). A better understanding of the dominant heating sources for the dust in galaxies as a function of type and luminosity should develop following multiwavelength studies of galaxies.

However, prior to the comparison of infrared observations of galaxies with those at other wavelengths, one must be assured that the infrared measurements are not only as sensitive as possible but that they also report the total emission of galaxies. The flux densities reported in the Point Source Catalog (1985, hereafter PSC) represent the total flux density for galaxies smaller than a few arcminutes in size. For galaxies larger than 8′, Rice *et al.* (1988) have produced a catalog of total flux densities based on *IRAS* surface brightness

[1]Department of Physics and Astronomy and Five College Radio Astronomy Observatory, University of Massachusetts, Amherst.
[2]Alfred P. Sloan Research Fellow.
[3]Astronomy Department, California Institute of Technology.
[4]Infrared Processing and Analysis Center, California Institute of Technology.

TABLE 1

Galaxy Properties

Name	UGC	R. A. (1950.0)	Decl. (1950.0)	Type	$V_\odot$ (km s^{-1})	V_{LG} (km s^{-1})	B_T^0	D_{25}	Alternative References
NGC 7814	00008	$00^h00^m41^s.1$	+15°52′03″	Sab	1047	1249	10.79	6′.3	
NGC 7817	00019	00 01 24.9	+20 28 18	Sbc	1208	1424	12.70	3.7	3
NGC 0023	00089	00 07 19.3	+25 38 50	Sa	4568	4793	12.33	2.3	
NGC 0157	...	00 32 14.4	−08 40 18	Sbc	1657	1749	10.67	4.3	1
NGC 185	00396	00 36 12.0	+48 03 50	E0-1	−245	4	9.51	11.5	
NGC 205	00426	00 37 38.7	+41 24 44	E0-1	−239	1	8.44	17.4	
NGC 253	...	00 45 07.8	−25 33 42	Sc	249	259	7.40	25.1	1
NGC 278	00528	00 49 14.8	+47 16 43	Sb	642	884	10.96	2.2	
NGC 520	00966	01 21 59.4	+03 32 13	Pec	2168	2272	11.55	4.8	
NGC 628	01149	01 34 00.7	+15 31 55	Sc	655	793	9.48	10.2	
NGC 660	01201	01 40 20.7	+13 23 32	Sa	855	981	12.31	9.1	3,4
NGC 695	01315	01 48 27.4	+22 20 10	S0	9769	9919	13.40	0.7	3,4
NGC 828	01655	02 07 07.0	+38 57 23	Sa	5430	5612	12.48	3.2	4
NGC 834	01672	02 08 00.6	+37 25 56	S	4553	4731	12.51	1.2	2,3,4,5
NGC 864	01736	02 12 49.8	+05 46 10	Sc	1564	1635	11.19	4.6	
NGC 877	01768	02 15 15.3	+14 19 01	Sbc	4016	4117	12.11	2.3	
NGC 891	01831	02 19 25.2	+42 07 18	Sb	524	706	9.83	13.5	
NGC 972	02045	02 31 16.6	+29 05 35	I0	1532	1670	11.53	3.6	
NGC 992	02103	02 34 35.7	+20 52 56	S?	4136	4245	13.09	0.9	2,3,4,5
NGC 1022	...	02 36 04.2	−06 53 24	Sa	1503	1505	11.85	2.5	1
NGC 1055	02173	02 39 10.7	+00 13 45	Sb	1050	1077	10.79	7.6	
NGC 1068	02188	02 40 06.5	−00 13 32	Sb	1109	1134	9.17	6.9	
NGC 1084	...	02 43 31.8	−07 47 06	Sc	1413	1406	10.73	2.9	1
NGC 1097	...	02 44 11.4	−30 29 06	Sb	1320	1227	9.91	9.3	1
NGC 1156	02455	02 56 46.8	+25 02 21	Im	380	485	11.73	3.1	
NGC 1275	02669	03 16 29.9	+41 19 55	Pec	5218	5361	11.45	2.6	
IC 342	02847	03 41 58.6	+67 56 26	Scd	32	228	7.86	17.8	
UGC 2982	02982	04 09 43.3	+05 25 12	S	5320	5290	14.84	2.3	1,2,3,4,5
NGC 1530	03013	04 17 04.9	+75 10 48	Sb	2465	2666	12.50	4.9	3,4
NGC 1569	03056	04 26 05.8	+64 44 18	Im	−87	87	10.58	2.9	
NGC 1614	...	04 31 36.0	−08 40 54	Sc	4745	4643	13.15	1.3	1
NGC 1620	03103	04 34 03.9	−00 14 42	Sbc	3510	3437	12.82	3.0	3,4
NGC 2146	03429	06 10 40.1	+78 22 23	Sab	838	1028	10.52	6.0	
NGC 2339	03693	07 05 25.1	+18 51 42	Sbc	2423	2334	11.54	2.8	
NGC 2276	03740	07 10 22.0	+85 50 58	Sc	2369	2579	11.44	2.6	
NGC 2403	03918	07 32 05.5	+65 42 40	Scd	131	259	8.30	17.8	
NGC 2532	04256	08 07 03.1	+34 06 20	Sc	5245	5211	12.61	2.2	
NGC 2623	04509	08 35 25.3	+25 55 35	Pec	5435	5355	14.03	0.6	
NGC 2633	04574	08 42 35.7	+74 17 00	Sb	2141	2302	12.34	2.6	
NGC 2681	04645	08 49 58.0	+51 30 16	S0/a	710	760	10.79	3.8	
NGC 2775	04820	09 07 41.0	+07 14 35	Sab	1135	965	10.85	4.5	
Arp 55	04881	09 12 39.6	+44 32 20	Doub	11957	11971	14.63	1.0	1,2,3,4,5
NGC 2798	04905	09 14 09.5	+42 12 37	Sa	1708	1709	12.43	2.8	
NGC 2841	04966	09 18 34.9	+51 11 19	Sb	652	700	9.58	8.1	
NGC 2903	05079	09 29 19.9	+21 43 19	Sbc	569	467	9.05	12.6	
NGC 3034	05322	09 51 45.3	+69 55 11	I0	246	388	8.72	11.2	
NGC 3079	05387	09 58 35.4	+55 55 11	Sc	1137	1212	10.43	7.6	
NGC 3077	05398	09 59 21.9	+68 58 33	I0	10	148	10.28	4.6	
NGC 3156	05503	10 10 05.6	+03 22 42	S0	1135	955	12.48	2.1	1,3,4
NGC 3147	05532	10 12 39.3	+73 39 02	Sbc	2721	2881	11.07	4.0	
NGC 3184	05557	10 15 17.7	+41 40 28	Scd	589	593	10.18	6.9	
NGC 3221	05601	10 19 35.5	+21 49 19	Sc	3971	3877	13.65	3.3	3,4
Mrk 33	05720	10 29 22.9	+54 39 34	Im	1446	1519	13.25	1.1	
NGC 3310	05786	10 35 40.3	+53 45 45	Sbc	994	1063	10.90	3.6	
NGC 3344	05840	10 40 46.6	+25 11 10	Sbc	585	513	10.28	6.9	
Mrk 35	05860	10 42 16.5	+56 13 23	Sb	865	948	12.86	1.5	
NGC 3368	05882	10 44 06.9	+12 05 05	Sab	905	773	9.79	7.1	
NGC 3437	05995	10 49 52.8	+23 12 01	Sc	1119	1041	12.06	2.6	4
NGC 3504	06118	11 00 28.1	+28 14 35	Sab	1529	1479	11.52	2.7	
NGC 3521	06150	11 03 15.1	+00 13 58	Sbc	815	640	9.26	9.6	
NGC 3556	06225	11 08 36.8	+55 56 33	Scd	685	772	10.00	8.3	
NGC 3623	06328	11 16 18.6	+13 22 00	Sa	780	666	9.59	10.0	
NGC 3627	06346	11 17 37.9	+13 16 08	Sb	697	583	9.26	8.7	
NGC 3628	06350	11 17 39.6	+13 51 48	Sb	839	728	9.47	14.8	
NGC 3690	06472	11 25 44.2	+58 50 23	Sm	2999	3104	...	2.4	4
NGC 3893	06778	11 46 01.1	+48 59 20	Sc	968	1034	10.73	4.4	
NGC 3992	06937	11 46 01.0	+53 39 13	Sbc	1059	1149	10.22	7.6	
NGC 4030	06993	11 57 50.3	−00 49 22	Sbc	1407	1255	12.09	4.3	4
NGC 4038	...	11 59 19.2	−18 35 06	Sm	1658	1447	10.88	2.6	1

TABLE 1—*Continued*

Name	UGC	R. A. (1950.0)	Decl. (1950.0)	Type	$V_{\odot}$ (km s^{-1})	V_{LG} (km s^{-1})	B_T^0	D_{25}	Alternative References
NGC 4064	07054	$12^h01^m37.3^s$	+18°43′16″	Sa	1026	959	11.71	4.5	
NGC 4088	07081	12 03 03.1	+50 49 13	Sbc	742	822	10.60	5.8	
NGC 4102	07096	12 03 51.6	+52 59 23	Sb	896	986	11.91	3.2	
NGC 4192	07231	12 11 15.4	+15 10 23	Sab	−129	−206	10.29	9.6	
NGC 4194	07241	12 11 41.7	+54 48 21	Im	2528	2629	12.55	2.5	
NGC 4212	07275	12 13 06.4	+14 10 45	Sbc	2027	1947	11.54	3.0	
NGC 4216	07284	12 13 20.3	+13 25 38	Sb	15	−69	10.26	8.3	
NGC 4236	07306	12 14 21.8	+69 44 36	Sdm	−1	160	9.32	18.6	
NGC 4254	07345	12 16 16.9	+14 41 46	Sc	2400	2324	10.18	5.4	
NGC 4258	07353	12 16 29.7	+47 34 55	Sbc	465	537	8.45	18.2	
NGC 4274	07377	12 17 20.2	+29 53 33	Sab	722	715	10.69	6.9	
NGC 4273	07380	12 17 22.3	+05 37 27	Sc	2302	2188	11.96	2.3	
NGC 4293	07405	12 18 41.1	+18 39 36	S0/a	882	825	10.77	6.0	
NGC 4294	07407	12 18 44.8	+11 47 18	Scd	415	328	12.10	3.1	
NGC 4298	07412	12 19 00.4	+14 53 03	Sc	1116	1042	11.70	3.2	
NGC 4299	07414	12 19 08.0	+11 46 53	Sdm	212	125	12.66	1.7	
NGC 4303	07420	12 19 21.4	+04 44 58	Sbc	1599	1483	9.97	6.0	
NGC 4312	07442	12 19 59.4	+15 48 58	Sab	153	83	12.27	4.7	3,4
NGC 4321	07450	12 20 23.2	+16 06 00	Sbc	1610	1543	9.86	6.9	
NGC 4380	07503	12 22 49.6	+10 17 33	Sb	971	879	13.02	3.7	4
NGC 4383	07507	12 22 53.8	+16 44 48	Sa	1710	1646	11.90	2.2	3,4
NGC 4388	07520	12 23 14.8	+12 56 18	Sb	2614	2535	11.17	5.1	
NGC 4394	07523	12 23 24.7	+18 29 30	Sb	772	717	11.51	3.9	
NGC 4402	07528	12 23 35.8	+13 23 22	Sb	234	156	13.02	4.1	3,4
NGC 4414	07539	12 23 58.2	+31 30 05	Sc	715	718	10.58	3.6	
NGC 4418	07545	12 24 20.3	−00 36 09	Sa	2045	1910	13.87	1.4	4,5
NGC 4419	07551	12 24 25.1	+15 19 28	Sa	−243	−312	11.07	3.4	3,4
NGC 4424	07561	12 24 39.0	+09 41 51	Sa	450	358	11.84	3.7	
NGC 4438	07574	12 25 13.5	+13 17 11	S0/a	259	182	10.39	9.3	
NGC 4449	07592	12 25 45.2	+44 22 15	Im	200	262	9.51	5.1	
NGC 4450	07594	12 25 58.0	+17 21 40	Sab	2048	1990	10.62	4.8	
NGC 4490	07651	12 28 10.5	+41 54 56	Sd	577	629	9.77	5.9	
NGC 4486	07654	12 28 17.8	+12 39 58	E+	1257	1180	9.35	7.2	
NGC 4501	07675	12 29 28.1	+14 41 50	Sb	2057	1989	9.86	6.9	
NGC 4526	07718	12 31 30.4	+07 58 33	S0	450	355	10.18	7.2	
NGC 4527	07721	12 31 35.5	+02 55 45	Sbc	1730	1614	10.73	6.3	
NGC 4532	07726	12 31 46.7	+06 44 43	Im	2159	2059	11.76	2.9	
NGC 4535	07727	12 31 47.9	+08 28 25	Sc	1946	1853	10.35	6.8	
NGC 4536	07732	12 31 53.5	+02 27 50	Sbc	1927	1810	10.50	7.4	
NGC 4540	07742	12 32 19.9	+15 49 41	Scd	1286	1224	12.24	2.0	3,4
NGC 4548	07753	12 32 55.1	+14 46 20	Sb	468	403	10.71	5.4	
NGC 4565	07772	12 33 51.8	+26 15 50	Sb	1136	1122	9.49	16.2	
NGC 4567	07777	12 34 01.1	+11 32 01	Sbc	2199	2121	11.75	3.0	
NGC 4569	07786	12 34 18.7	+13 26 18	Sab	−312	−382	9.80	9.6	
NGC 4571	07788	12 34 25.5	+14 29 33	Sd	342	276	13.37	3.8	3,4
NGC 4579	07796	12 35 12.6	+12 05 40	Sb	1805	1730	10.33	5.4	
NGC 4594	...	12 37 22.8	−11 21 00	Sa	1128	963	8.74	8.9	1
NGC 4602	...	12 38 01.8	−04 51 30	Sbc	2559	2417	...	3.6	1,3
NGC 4605	07831	12 37 47.5	+61 53 00	Sc	148	286	10.41	5.5	
NGC 4631	07865	12 39 41.5	+32 48 54	Sd	620	638	9.03	15.1	
NGC 4639	07884	12 40 21.7	+13 31 56	Sbc	963	897	11.90	2.9	
NGC 4647	07896	12 41 01.1	+11 51 21	Sc	1358	1286	11.64	3.0	
NGC 4651	07901	12 41 12.5	+16 40 05	Sc	794	742	10.99	3.8	
NGC 4654	07902	12 41 25.7	+13 23 58	Scd	1036	970	10.75	4.7	
NGC 4656	07907	12 41 32.8	+32 27 00	Sm	645	662	10.00	13.8	
NGC 4666	07926	12 42 35.1	−00 11 14	Sc	1516	1395	10.96	4.5	
NGC 4689	07965	12 45 15.3	+14 02 13	Sbc	1620	1559	12.56	4.0	3,4
NGC 4698	07970	12 45 51.8	+08 45 37	Sab	946	864	10.99	4.3	
NGC 4710	07980	12 47 09.0	+15 26 15	S0	1129	1076	11.25	5.1	
NGC 4713	07985	12 47 25.6	+05 34 58	Sd	664	570	11.86	2.8	
NGC 4725	07989	12 47 59.9	+25 46 20	Sab	1138	1131	9.64	11.0	
NGC 4736	07996	12 48 32.4	+41 23 28	Sab	269	329	8.58	11.0	
NGC 4746	08007	12 49 25.2	+12 21 18	Sb	1779	1714	12.66	2.5	4
NGC 4808	08054	12 53 17.0	+04 34 28	Scd	773	679	12.04	2.7	4
Mrk 231	08058	12 54 05.0	+57 08 41	Sc	12430	12556	13.86	1.7	
NGC 4900	08116	12 58 06.4	+02 46 11	Sc	1043	945	11.87	2.3	
NGC 5033	08307	13 11 09.7	+36 51 30	Sc	907	961	10.18	10.5	
NGC 5055	08334	13 13 34.9	+42 17 55	Sbc	509	587	8.93	12.3	
IC 883	08387	13 18 16.8	+34 23 54	Im	6894	6942	14.47	1.7	1,4
NGC 5194	08493	13 27 46.9	+47 27 16	Sbc	460	565	8.62	11.0	

TABLE 1—*Continued*

Name	UGC	R. A. (1950.0)	Decl. (1950.0)	Type	$V_{\odot}$ (km s^{-1})	V_{LG} (km s^{-1})	B_T^0	D_{25}	Alternative References
NGC 5236	...	13^{h}34^{m}10.2^s	−29°36′48″	Sc	518	337	7.85	11.2	1
NGC 5248	08616	13 35 02.4	+09 08 23	Sbc	1146	1102	10.49	6.5	
NGC 5256	08632	13 36 15.2	+48 31 53	Pec	8257	8371	13.85	1.5	4
Mrk 273	08696	13 42 51.0	+56 08 18	Pec	11390	11533	13.98	1.3	1
NGC 5457	08981	14 01 26.6	+54 35 25	Scd	241	388	7.96	26.9	
NGC 5775	09579	14 51 26.8	+03 44 51	Sc	1582	1581	11.49	4.3	
NGC 5866	09723	15 05 07.8	+55 57 16	S0+	692	874	10.39	5.3	
NGC 5907	...	15 14 36.6	+56 30 24	Sc	592	780	10.08	12.3	
NGC 5936	09867	15 27 39.7	+13 09 40	Sb	4029	4095	12.67	1.6	3,4
Arp 220............	09913	15 32 47.3	+23 40 06	Pec	5400	5508	14.06	2.0	2,3,4,5
NGC 6207	10521	16 41 17.8	+36 55 32	Sc	870	1066	11.61	3.0	
NGC 6240	10592	16 50 27.6	+02 29 06	I0	7503	7597	13.92	2.2	1,4
NGC 6286	10647	16 57 45.1	+59 00 43	Sb	5600	5838	13.87	1.6	3,4
NGC 6384	10891	17 29 59.0	+07 05 43	Sbc	1660	1801	10.47	6.0	
NGC 6503	11012	17 49 58.7	+70 09 26	Scd	62	315	10.15	6.2	
NGC 6509	11075	17 56 58.5	+06 17 20	Sc	1816	1973	12.34	1.6	2,3,4,5
NGC 6574	11144	18 09 34.7	+14 58 03	Sbc	2315	2509	11.95	1.5	
NGC 6643	11218	18 21 13.3	+74 32 43	Sc	1482	1736	11.07	3.9	
NGC 6701	11348	18 42 35.5	+60 36 08	Sa	3950	4223	12.38	1.8	3,4
NGC 6921	11570	20 26 21.0	+25 33 24	S0/a	4317	4590	13.11	1.2	1,4
NGC 6946	11597	20 33 48.8	+59 58 50	Scd	46	338	8.49	11.0	
NGC 7217	11914	22 05 37.6	+31 06 53	Sab	946	1227	10.49	3.7	
NGC 7331	12113	22 34 47.7	+34 09 35	Sbc	826	1105	9.51	10.7	
NGC 7469	12332	23 00 44.4	+08 36 19	Sa	4894	5102	12.16	1.8	
NGC 7479	12343	23 02 26.8	+12 03 06	Sc	2385	2604	11.33	4.1	
NGC 7541	12447	23 12 10.3	+04 15 43	Sbc	2672	2860	11.85	3.5	
NGC 7625	12529	23 18 00.6	+16 57 15	Sa	1637	1864	12.47	1.8	
NGC 7674	12608	23 25 24.4	+08 30 06	Sbc	8850	9047	13.32	1.2	4
NGC 7741	12754	23 41 22.7	+25 47 53	Scd	779	1018	11.52	4.0	
NGC 7771	12815	23 48 52.3	+19 50 08	Sa	4290	4510	12.51	2.7	
IIZw 40............	...	05 53 04.8	+03 23 06	cI	806	689	15.60	0.3	1
IIZw 70............	...	14 48 54.0	+35 47 00	Pec	1147	1262	14.21	0.8	1
IIIZw 102	12529	23 18 00.6	+16 57 15	Sa	1637	1864	12.47	1.8	
DDO 47	...	07 39 03.0	+16 55 06	dI	266	155	13.10	4.7	1,4,6
DDO 50	...	08 13 43.2	+70 52 18	dI	158	305	10.76	7.6	1,4,6
DDO 135	...	12 31 17.4	+15 26 36	dI	263	200	14.23	2.6	1,4,6
DDO 155	...	12 56 10.2	+14 29 12	dI	222	171	14.47	1.2	1,4,6
DDO 210	...	20 44 07.8	−13 02 00	dI	−130	13	15.34	2.1	1,6
DDO 216	...	23 26 03.0	+14 28 18	dI	−178	38	11.90	4.6	1,4,6
DDO 218	...	23 32 22.2	+17 57 00	dI	1395	1618	13.76	1.5	1,4,6
LGS 003...........	...	01 01 12.0	+21 37 00	dI	−280	...	15.52	2.0	1,6
M081DWA........	...	08 18 42.0	+71 11 36	dI	113	...	16.60	1.7	1,6
Mrk 0331	...	23 48 53.4	+20 18 30	Sa	5386	5608	...	0.9	1

NOTES.—The columns are as follows:

Col. (1).—Galaxy name—NGC, IC, Mrk, DDO, Arp, or Zw designation.

Col. (2).—UGC designation.

Cols. (3)–(4).—Right ascension and declination from Dressel and Condon (1976), unless alternate reference listed in column (10).

Col. (5).—Morphological type from RC2 unless alternate reference noted in column (10).

Col. (6).—Heliocentric velocity, $V_{\odot}$, from RC2 unless alternate reference noted in column (10).

Col. (7).—Velocity corrected to the center of the Local Group from RC2, unless alternate reference noted in column (10), assuming $V_{LG} = V_{\odot} + \Delta V = V_{\odot} + 300 \sin(l) \cos(b)$.

Col. (8).—Total blue magnitude, B_{T^0}, corrected for Galactic and internal absorption from RC2, unless alternate reference noted in column (10).

Col. (9).—Optical diameter measured out to the 25 mag arcsec^{-2} isophote from RC2 unless alternate reference listed in column (10).

Col. (10).—Alternative references: (1) Coordinates from RC2, UGC, Cataloged Galaxies in the *IRAS Survey* (1985), or references in Tacconi and Young (1987). (2) Morphological type from UGC. (3) $V_{\odot}$ from UGC, Huchra (1985), Huchtmeier *et al.* (1983), Sanders *et al.* (1986), Kenney (1987), or Young *et al.* (1988). (4) B_T from UGC corrected for Galactic absorption as in RC2, or B_{T^0} from de Vaucouleurs, de Vaucouleurs, and Buta (1981). (5) Blue optical diameter from UGC. (6) $V_{\odot}$, distance, and D_{25} from references in Tacconi and Young (1987).

maps, in which extended emission associated with each object is included. Here, we report the *IRAS* data for 182 galaxies of a range of sizes and present an analysis of several methods used to determine total flux densities. Finally, we compare the IR luminosities and dust masses with the interstellar gas masses of these galaxies.

II. GALAXY SAMPLE

The 182 galaxies for which we have analyzed the *IRAS* data are primarily a sample of galaxies we selected for observation of their molecular content as part of the Five College Radio Astronomy Observatory (FCRAO) Extragalactic CO Survey. The ongoing CO Survey consists of observations at

2.6 mm of a complete, magnitude-limited sample of spiral and irregular galaxies selected on the basis of their declination and optical or infrared properties ($\delta > -20°, B_{T^0} < 12$, or $S_{100} > 10$ Jy, or $S_{60} > 5$ Jy. Table 1 lists the 182 galaxies whose total *IRAS* flux densities are presented in this paper. The columns of Table 1 are as follows: column (1), the NGC, IC, Mrk, or DDO number; column (2), the UGC number (Nilson 1973); columns (3)–(4), the right ascension and declination (Dressel and Condon 1976); column (5), the morphological type (de Vaucouleurs, de Vaucouleurs, and Corwin 1976, hereafter RC2); columns (6)–(7), the recessional velocities with respect to the Sun and to the Local Group; column (8), the total blue magnitude from RC2; column (9), the optical (blue light) angular diameter measured to a surface brightness level of 25 mag arcsec^{-2} from RC2; and column (10), reference notes.

III. *IRAS* DATA, REDUCTION, AND ANALYSIS

a) *Data Processing*

The *IRAS* data have been accessed from the PSC and by the following methods. For 69 of the sample galaxies, two-dimensional spatial maps were constructed by adding *IRAS* all-sky survey data (called Survey Co-adds, hereafter SCs), while for 12 galaxies the maps were constructed by co-adding *IRAS* pointed observations (called Additional Observations, hereafter AOs). These 81 galaxies have optical sizes ranging from 2′ to 25′, with 36 galaxies larger than 8′, 21 galaxies between 5′ and 8′, 18 galaxies between 3′ and 5′, and six galaxies smaller than 3′.

An alternative method for deriving total flux densities, used for 158 galaxies, was to co-add the survey data in one dimension and produce an emission profile along the *IRAS* scanning direction (called Addscan, hereafter AS). Because Addscan flux densities were derived for most of the galaxies in the sample, we were able to compare these flux densities with those listed in the PSC Survey and with those derived from AO co-added maps, and thereby check the relative calibration of the flux densities derived by each method. We have found that Survey co-adds tend to underestimate the 60 μm flux by 15%–20% relative to Addscan and the PSC as discussed in § III*b*.

i) *Map Processing*

The various steps required to produce *IRAS* surface brightness and point source filtered spatial maps are described in detail in Young *et al.* (1985) and in Rice *et al.* (1988). For galaxies unresolved by *IRAS*, total flux densities were derived from point source filtered maps. Alternatively, for the galaxies observed as extended sources, total flux densities were derived from each surface brightness map by integrating the emission in an elliptical aperture matched to the galaxy inclination and position angle. Flux densities were typically integrated out to a surface brightness of 10–20 mJy arcmin^{-2} depending on the local noise level.

The uncertainties in flux densities determined from surface brightness maps are typically of order 20%. For the 36 galaxies larger than 8′, the flux densities in each band agree with those reported by Rice *et al.* (1988) to within the stated uncertainty.

ii) *Addscan Processing*

The Addscan profiles were measured using the IPAC scan processing and integration tool, Scanpi, described in the *IPAC User's Guide* to determine the flux densities for all but the largest galaxies in the sample. Throughout this study we have used flux densities derived from the median co-added scan in each band. The rms noise levels, calculated over the regions where baselines were fitted to the data, were found to be roughly 20, 30, 50, and 100 mJy at 12, 25, 60, and 100 μm, respectively. These flux densities are more reliable than those in the PSC since they are based on more *IRAS* data and since extended emission is included. In addition, more galaxies are detected because of the greater sensitivity. The flux density uncertainties are of order 10%.

The profile widths in the in-scan direction, measured at 50% of the peak [$W(50)$], were used to determine which sources were extended; peak flux densities were used for point sources, and integrated flux densities were used for the extended sources. Based on the distribution of $W(50)$ values for profiles with signal-to-noise ratios greater than 20 in a given band, we selected 0′.75, 0′.75, 1′.5, and 3′.0 at 12, 25, 60, and 100 μm, respectively, as the maximum profile half-widths for point sources. All galaxies with profile half-widths greater than these values were classified as extended sources.

b) *Relative Calibration of PSC, Addscan, and Survey Co-Adds*

In order to check the relative calibration of the flux densities derived from the PSC, Addscan, and co-added Survey data, we have compared the Addscan flux densities in each band with signal-to-noise ratios greater than 20 with the PSC values for point sources and with the SCs for extended sources. For the galaxies which were found to be *IRAS* point sources, the Addscan flux densities agree with the PSC at 12 and 60 μm, but are 15% too high at 25 and 100 μm. The overestimation of Addscan flux densities relative to the PSC is pointed out in the *IPAC User's Guide* (§ XI.H.2.d) and in a recent IPAC Newsletter. For the subset of galaxies which are extended, we find that Addscan overestimates the flux densities by ~10%–15% in all four bands relative to co-added Survey data. In addition, SCs at 60 μm are low by 20% relative to Addscan and the PSC.

The results of our flux density comparison are given in Table 2. All of the flux densities reported in this paper have been scaled by the appropriate values listed in Table 2 to produce Survey co-add and Addscan flux densities (using the 1986 February calibration) on the same scale as the PSC.

c) *Flux Density Results*

Table 3 lists the final scaled flux densities in each band for the galaxies in our sample. For the 38 galaxies which are in common with the Virgo sample of Helou *et al.* (1988), we find agreement within the stated uncertainties for all galaxies or galaxy pairs. The entries in Table 3 are as follows:

Column (1).—Galaxy NGC, UGC, IC, Mrk, or DDO designation.

TABLE 2

RESULTS OF PSC, ADDSCAN, AND SURVEY CO-ADD COMPARISONS[a]

FLUX COMPARISON	FLUX DENSITY RATIO[b] 12 μm	25 μm	60 μm	100 μm
S(PSC)/S(Addscan)[c]	1.00 ± 0.06(25)	0.85 ± 0.04(5)	0.98 ± 0.02(58)	0.87 ± 0.01(69)
S(SCI)/S(Addscan)[d]	0.89 ± 0.03(43)	0.89 ± 0.04(43)	0.83 ± 0.03(33)	0.89 ± 0.03(27)
S(PSC)/S(SCI)[e]	1.12 ± 0.08	0.96 ± 0.06	1.18 ± 0.05	0.98 ± 0.04

[a] Flux densities derived from Addscan using the 1986 February calibration are compared with the 1985 version of the PSC.

[b] Flux density ratios and the uncertainties in the mean are given. The number of galaxies used to determine each mean is given in parentheses.

[c] Addscan *peak* flux densities are used for sources whose Addscan profiles have half-widths less than the instrumental resolution of 0′.75, 0′.75, 1′.5, and 3′.0 at 12, 25, 60, and 100 μm, respectively. Kenney (1987) has shown that the ratio S(PSC)/S(Addscan) is similar if one uses larger cutoffs of 0′.8, 0′.8, 1′.6, and 3′.1, respectively, in the four bands in order to include more galaxies in the derivation of the ratio.

[d] Addscan *integrated* flux density values are used for galaxies whose Addscan profiles have half-widths ≥ 0′.8, 0′.8, 1′.6, and 3′.1 at 12, 25, 60, and 100 μm, respectively, and smaller than 2′.0, 2′.0, 2′.5, and 3′.5.

[e] Computed by dividing S(PSC)/S(Addscan) by S(SCI)/S(Addscan).

TABLE 3

FLUX DENSITIES

Name	S_{12} (Jy)	S_{25} (Jy)	S_{60} (Jy)	S_{100} (Jy)	Source	T_d (K)	S_{CO} (Jy km s^{-1})	S_{HI} (Jy km s^{-1})	$F_{H\alpha}$ (10^{-12} ergs cm^{-2} s^{-1})
NGC 7814	0.11	0.20	1.8	5.8	AS	30.5	< 300	20.6	...
	...	...	...	...	PS				
NGC 7817	0.64	0.57	5.4	14.9	AS	32.0	320	14.7	...
	0.49	0.58	5.1	15.1	PS				
NCG 23	0.64	1.23	9.9	14.9	AS	40.5	220	8.9	...
	0.47	1.15	9.0	15.8	PS				
NGC 157	1.88	2.22	19.3	42.7	SV	34.7	...	78.5	4.7
	< 0.61	0.69:	12.6	36.9	PS				
NGC 185	< 0.06	0.06	0.3	1.4	AS	27.9	...	3.6	...
	< 0.29	< 0.25	< 0.4	2.1	PS				
NGC 205	0.11	0.10	0.5	3.5	AS	24.7	...	0.2	...
	< 0.25	< 0.24	< 0.6	3.1	PS				
NGC 253	62.04	147.34	1157.2	1760.2	SV	40.3	19600	1743.0	...
	20.52	117.08	758.6	1044.8	PS				
NGC 278	1.82	2.44	26.6	41.9	AS	39.7	...	32.1	6.8
	1.25	2.00	23.4	44.2	PS				
NGC 520	0.87	2.99	30.6	45.7	AS	40.7	1120	26.0	26.0a
	0.78	2.85	31.2	47.4	PS				
NGC 628	3.03	2.81	25.5	67.4	SV	32.5	...	529.7	12.9
	< 0.25	< 0.40	3.0	11.8	PS				
NGC 660	4.08	9.14	80.9	105.1	SV	43.3	...	185.5	140.0a
	2.02	7.12	65.0	102.4	PS				
NGC 695	0.60	0.91	8.3	14.0	AS	38.5	220	< 3.0	...
	0.48	0.82	8.0	13.1	PS				
NGC 828	0.79	1.08	12.3	24.0	AS	36.4	430	8.5	...
	0.75	1.03	10.9	25.7	PS				
NGC 834	0.47	0.77	6.5	12.7	AS	36.3	150	5.5	...
	0.39	0.76	6.4	13.2	PS				
NGC 864	0.69	0.36	4.6	10.0	AS	35.0	300	94.4	...
	< 0.25	0.37	3.1	9.6	PS				
NGC 877	0.95	1.36	12.3	23.0	AS	37.1	330	30.0	...
	0.41	0.60	8.9	23.7	PS				
NGC 891	5.76	7.06	75.7	183.7	SV	33.5	4690	182.3	...
	0.93	0.85:	34.1	146.3	PS				
NGC 972	3.31	3.25	34.8	58.4	AS	38.7	...	15.8	...
	1.58	2.62	29.9	63.6	PS				
NGC 992	0.63	1.69	11.7	15.8	AS	42.6	...	12.8	...
	0.56	1.22	10.0	16.4	PS				
NGC 1022	0.77	3.30	20.7	25.3	AS	44.6	...	4.3	0.7
	0.80	3.28	19.9	26.7	PS				

TABLE 3—*Continued*

Name	S_{12} (Jy)	S_{25} (Jy)	S_{60} (Jy)	S_{100} (Jy)	Source	T_d (K)	S_{CO} (Jy km s^{-1})	S_{HI} (Jy km s^{-1})	$F_{H\alpha}$ (10^{-12} ergs cm^{-2} s^{-1})
NGC 1055	2.37	2.76	24.3	58.2	AS	33.6	…	91.8	…
	1.23	1.66	20.5	59.3	PS				
NGC 1068	45.40	89.20	207.8	235.6	AS	46.3	4670	51.4	82.0a
	38.30	86.83	185.6	238.7	PS				
NGC 1084	2.12	3.23	29.7	53.7	AS	37.6	…	60.5	6.6
	1.26	2.30	25.6	54.0	PS				
NGC 1097	3.22	7.64	50.8	108.9	SV	35.2	…	137.3	…
	1.85	5.83	45.5	82.5	PS				
NGC 1156	0.29	0.59	6.6	10.4	AS	39.7	…	76.4	2.3:
	< 0.25	0.48	5.2	10.2	PS				
NGC 1275	1.11	3.26	7.2	6.5	AS	52.2	…	…	…
	1.03	3.63	7.1	7.8	PS				
IC 342	27.12	44.68	272.1	592.3	SV	34.9	24400	3817.0	…
	3.80	18.76	85.2	126.0	PS				
UGC 2982	0.59	0.74	8.9	17.1	AS	36.7	…	…	…
	0.56	0.81	8.3	15.7	PS				
NGC 1530	0.79	1.06	10.3	24.4	AS	33.8	450	34.4	…
	0.37	0.77	8.4	23.5	PS				
NGC 1569	1.21	8.26	56.1	48.2	AS	53.9	36	95.0	25.0
	0.68	6.87	46.3	50.7	PS				
NGC 1614	1.60	6.97	33.2	33.5	AS	49.2	270	3.7	…
	1.39	7.59	33.2	31.6	PS				
NGC 1620	0.33	0.30	1.9	5.4	AS	31.8	…	22.3	…
	< 0.25	< 0.25	1.3	5.0	PS				
NGC 2146	7.51	18.43	151.8	183.4	AS	44.9	2620	124.5	32.0a
	5.84	17.31	141.3	185.7	PS				
NGC 2339	0.84	2.29	20.1	31.4	AS	39.9	870	21.7	3.2
	0.53	2.12	18.7	31.5	PS				
NGC 2276	1.24	1.55	14.1	28.7	AS	35.9	780	20.0	…
	0.59	1.14	11.6	28.7	PS				
NGC 2403	4.15	5.89	62.6	129.2	SV	35.7	560	1628.0	…
	< 0.28	1.30	11.5	54.6	PS				
NGC 2532	0.51	0.86	4.5	10.8	AS	33.7	120	13.0	…
	< 0.34	0.74	3.6	10.0	PS				
NGC 2623	0.32	1.50	25.2	25.0	AS	49.8	180	1.4	…
	0.36:	1.75	24.1	27.5	PS				
NGC 2633	0.91	2.37	15.8	25.0	AS	39.7	330	20.6	…
	0.68	2.33	15.9	26.3	PS				
NGC 2681	0.32	0.54	6.8	11.2	AS	39.0	…	…	…
	< 0.35	0.59	7.0	11.0	PS				
NGC 2775	0.42	0.54	2.7	10.0	AS	29.1	550	6.5	…
	0.25	0.28	1.7	10.1	PS				
Arp 55	0.28	0.67	6.5	9.1	AS	41.8	180	…	…
	< 0.25	0.60	5.9	9.8	PS				
NGC 2798/99	0.84	3.02	21.0	29.2	AS	41.9	330	10.3	…
	0.77	3.13	22.5	28.4	PS				
NGC 2841	1.40	1.15	6.3	23.7	SV	29.0	2110	137.2	…
	< 0.25	< 0.25	2.4	13.5	PS				
NGC 2903	5.90	8.39	67.6	116.0	SV	38.3	…	208.5	…
	0.86	2.33	27.9	102.6	PS				
NGC 3034	79.67	304.31	1444.4	1418.6	SV	50.0	13600	536.1	320.0a
	53.21	273.98	1167.8	1145.1	PS				
NGC 3079	2.81	3.54	52.8	96.5	AS	37.4	2500	108.1	…
	1.25	2.04	42.5	87.6	PS				
NGC 3077	0.78	1.89	16.8	25.0	AS	40.7	…	296.0	…
	0.55	1.91	14.6	24.4	PS				
NGC 3156	0.10	0.18	0.2	0.7	AS	29.6	…	1.4	…
	…	…	…	…	PS				
NGC 3147	0.98	1.04	8.3	28.2	AS	30.0	1360	16.7	…
	0.53	0.62	6.6	24.0	PS				
NGC 3184	1.36	1.69	10.5	30.4	SV	31.6	…	129.0	…
	< 0.25	< 0.55	2.3	14.9	PS				
NGC 3221	0.62	0.90	8.0	18.6	AS	34.0	300	18.0	…
	0.48	0.70:	6.9	18.3	PS				
Mrk 33	0.22	0.99	4.5	5.8	AS	43.7	…	5.0	…
	< 0.26	0.98	4.7	5.3	PS				
NGC 3310	1.76	5.08	36.5	43.1	AS	45.4	140	78.6	12.3
	1.25	4.66	33.0	40.8	PS				

TABLE 3—*Continued*

Name	S_{12} (Jy)	S_{25} (Jy)	S_{60} (Jy)	S_{100} (Jy)	Source	T_d (K)	S_{CO} (Jy km s^{-1})	S_{HI} (Jy km s^{-1})	$F_{H\alpha}$ (10^{-12} ergs cm^{-2} s^{-1})
NGC 3344	1.07	1.37	9.9	26.0	AS	32.6	660	168.3	...
	< 0.25	0.57	4.5	20.1	PS				
Mrk 35	0.43	0.85	5.6	6.6	AS	45.1	25	11.6	...
	< 0.25	0.93	5.1	6.4	PS				
NGC 3368	1.10	0.53	11.1	26.7	AS	33.6	...	65.0	2.8
	0.45	< 0.56	9.0	26.7	PS				
NGC 3437	0.83	1.09	11.7	19.0	AS	39.2	190	41.5	...
	< 0.77	1.29	11.4	20.0	PS				
NGC 3504	1.21	3.86	23.3	33.8	AS	41.2	360	4.5	3.5
	1.05	3.74	18.9	32.1	PS				
NGC 3521	5.96	4.99	52.8	121.4	SV	34.2	4920	259.6	11.2:
	< 0.98	0.92:	27.0	83.7	PS				
NGC 3556	2.46	4.86	38.2	80.8	SV	35.4	1010	159.4	...
	0.61	1.80	23.3	60.1	PS				
NGC 3623	0.68	0.83	4.6	17.0	AS	29.2	< 680	15.1	...
	< 0.25	< 0.34	2.0	12.9	PS				
NGC 3627	5.47	8.22	66.5	141.5	SV	35.3	3680	39.9	11.5:
	0.72:	1.37:	33.7:	104.2	PS				
NGC 3628	3.71	5.83	56.9	117.5	SV	35.7	3190	265.4	...
	2.61	4.67:	48.0	101.7	PS				
NGC 3690	4.37	23.24	125.9	110.1	AS	53.3	510	< 5.9	...
	3.73	21.57	105.4	109.7	PS				
NGC 3893	1.64	1.64	16.0	36.0	AS	34.5	540	76.9	...
	0.83	1.14	13.6	34.2	PS				
NGC 3992	0.93	0.76	4.3	17.8	SV	28.1	...	81.8	...
	< 0.30	< 0.25	0.8:	9.0	PS				
NGC 4030	1.56	2.33	19.1	47.3	AS	33.2	...	67.4	...
	0.81	1.27	16.4	45.4	PS				
NGC 4038/39	2.37	6.31	43.5	75.0	AS	38.3	1340	49.8	...
	1.22	3.93	38.9	74.7	PS				
NGC 4064	0.21	0.28	3.5	7.1	AS	36.1	93	< 2.6	...
	< 0.29	< 0.36	3.5	6.8	PS				
NGC 4088	2.21	3.36	28.0	56.2	AS	36.1	...	108.0	...
	0.55	1.14	17.0	50.6	PS				
NGC 4102	1.86	6.67	50.9	69.5	AS	42.3	...	11.6	...
	1.46	6.87	47.0	67.3	PS				
NGC 4192	1.11	1.17	8.4	21.8	AS	32.7	940	89.2	...
	< 0.33	< 0.45	5.0	18.4	PS				
NGC 4194	1.06	4.30	25.4	24.5	AS	50.5	150	5.6	...
	0.86	4.39	22.5	25.2	PS				
NGC 4212	0.95	0.73	7.3	15.6	AS	35.3	510	< 3.0	2.0
	< 0.41	0.65:	6.6:	16.1	PS				
NGC 4216	0.75	2.07	3.7	13.8	AS	29.1	620	36.9	...
	< 0.34	< 0.31	< 0.9	7.4	PS				
NGC 4236	0.09	0.08	5.2	9.1	SV	38.1	...	582.7	...
	< 0.25	0.29:	1.6	3.9	PS				
NGC 4254	4.49	5.09	40.7	88.6	AS	34.9	3000	103.4	12.3
	1.05	1.36	22.8	71.3	PS				
NGC 4258	3.59	3.31	27.4	77.2	AO	31.8	...	457.5	...
	...	...	...	...	PS				
NGC 4274	0.50	0.63	4.4	14.5	AS	30.2	...	9.2	...
	< 0.36	0.54	4.1	14.0	PS				
NGC 4273	0.86	1.63	10.0	21.5	AS	35.2	...	17.7	...
	0.60	1.18	9.7	21.1	PS				
NGC 4293	0.24	0.55	4.8	10.2	AS	35.4	270	...	...
	< 0.25	0.54:	4.5	10.3	PS				
NGC 4294	< 0.18	< 0.06	3.0	5.5	AS	37.3	< 60	31.4	2.0
	< 0.25	< 0.31	2.7	5.5	PS				
NGC 4298/302	0.62	0.69	8.3	29.1	SV	29.7	660	12.9	1.0
	0.43:	0.52:	4.1	19.2	PS				
NGC 4299	< 0.06	0.17	2.4	4.7	AS	36.3	...	15.0	2.0
	< 0.25	< 0.40	2.5	4.8	PS				
NGC 4303	3.51	4.66	40.2	79.1	AS	36.3	2280	100.7	14.1
	< 0.49	< 0.61	23.2	60.6	PS				
NGC 4312	0.29	0.26	2.1	6.4	AS	31.1	160	...	...
	< 0.25	< 0.32	2.1	6.0	PS				
NGC 4321	2.79	3.17	26.9	65.2	AS	33.5	3340	48.1	8.9
	0.79	1.32	18.0	56.6	PS				
NGC 4380	< 0.08	< 0.06	0.7	2.9	AS	28.1	< 60	2.4	...
	< 0.57	< 0.31	0.6	3.1	PS				

TABLE 3—*Continued*

Name	S_{12} (Jy)	S_{25} (Jy)	S_{60} (Jy)	S_{100} (Jy)	Source	T_d (K)	S_{CO} (Jy km s^{-1})	S_{HI} (Jy km s^{-1})	$F_{H\alpha}$ (10^{-12} ergs cm^{-2} s^{-1})
NGC 4383	0.36	0.97	9.0	12.5	AS	42.0	...	...	...
	< 0.38	1.04	8.5	12.0	PS				
NGC 4388	1.16	3.25	10.9	17.7	AS	39.1	230	9.0	...
	1.00	3.57	10.7	17.3	PS				
NGC 4394	0.20	0.19	1.1	4.3	AS	29.0	280	7.0	...
	< 0.30	< 0.25	1.0	4.2	PS				
NGC 4402	0.55	0.69	5.0	16.1	AS	30.5	630	7.2	...
	0.53:	0.61	5.7	16.9	PS				
NGC 4414	3.25	3.60	31.5	70.1	AS	34.6	...	65.2	...
	1.55	1.90	25.8	67.2	PS				
NGC 4418	1.00	8.61	38.6	29.7	AS	57.6	...	...	...
	0.94	9.62	43.5	33.0	PS				
NGC 4419	0.63	1.41	7.8	15.6	AS	36.1	920	1.8	...
	0.55	1.46	7.7	17.3	PS				
NGC 4424	0.18	0.29	3.1	5.8	AS	36.9	56	3.3	...
	< 0.25	< 0.54	3.2	5.8	PS				
NGC 4438	< 0.13	0.15	3.8	10.5	AS	32.1	210	7.7	...
	< 0.25	< 0.27	4.0	10.4	PS				
NGC 4449	1.80	3.96	37.9	67.1	AO	37.9	150	788.2	25.7
	...	...	...	...	PS				
NGC 4450	< 0.14	< 0.04	2.0	7.5	AS	28.8	450	3.7	...
	< 0.25	< 0.25	1.2	6.8	PS				
NGC 4490/85	2.00	4.42	50.8	79.0	AS	40.0	280	367.5	...
	1.20	3.28	39.6	76.7	PS				
NGC 4486	0.41	0.15	0.4	0.4	AS	50.2	...	215.0	...
	< 0.48	< 0.34	0.5	<1.2	PS				
NGC 4501	2.37	2.57	20.7	60.3	AS	31.5	2220	34.3	3.2
	0.70	0.93	14.0	54.4	PS				
NGC 4526	0.58	0.61	6.1	14.6	AS	33.7	< 90	...	...
	< 0.33	0.59:	5.8	15.5	PS				
NGC 4527	2.55	2.96	36.0	61.9	AS	38.3	1800	94.3	...
	1.02	1.88	25.5	62.4	PS				
NGC 4532	0.33	1.03	8.7	15.3	AS	37.9	< 60	48.4	...
	< 0.50	0.86	8.8	15.2	PS				
NGC 4535	2.02	2.10	12.6	28.8	AS	34.2	1570	107.7	3.7
	< 0.25	< 0.70	6.4	20.9	PS				
NGC 4536	1.82	4.42	33.9	42.9	AS	43.9	740	71.7	3.3
	1.42:	3.49:	30.0	44.0	PS				
NGC 4540	0.34	0.97	2.4	5.7	AS	33.5	...	...	...
	< 0.29	< 0.46	1.3:	5.5	PS				
NGC 4548	0.61	0.39	2.3	9.9	AS	27.8	540	20.0	0.9:
	<1.82	< 0.25	1.2	7.8	PS				
NGC 4565	1.89	1.28	12.1	43.6	SV	29.5	...	242.2	...
	< 0.90	0.58:	5.9	24.7:	PS				
NGC 4567/68	1.75	2.73	21.9	57.3	SV	32.6	1050	21.7	...
	0.58	0.98	15.3:	46.6	PS				
NGC 4569	1.42	2.17	11.0	24.6	AS	34.6	1500	8.7	2.4
	< 0.35	0.89	7.1	22.7	PS				
NGC 4571	0.28	< 0.16	1.5	6.0	AS	28.7	380	13.1	0.8
	< 0.25	< 0.25	0.9	6.3	PS				
NGC 4579	0.69	0.67	6.0	18.7	AS	30.7	910	10.1	...
	< 0.38	< 0.33	4.5:	17.4	PS				
NGC 4594	1.22	0.61	5.8	21.6	SV	29.1	...	10.7	...
	< 0.57	0.43:	3.1	11.7	PS				
NGC 4602	0.57	0.56	5.2	12.6	AS	33.4	...	...	0.9:
	0.54	0.50:	5.0	13.2	PS				
NGC 4605	1.00	1.21	15.4	30.1	AS	36.4	190	51.7	...
	0.48	0.78	12.0	29.7	PS				
NGC 4631	5.10	8.80	90.7	170.4	SV	37.0	...	765.3	19.5
	1.82	3.01	51.2	118.6	PS				
NGC 4639	< 0.14	0.13	1.9	4.9	AS	32.7	< 70	18.8	...
	< 0.25	< 0.31	1.4	4.4	PS				
NGC 4647	1.24	0.84	5.8	16.1	AS	32.0	600	8.9	...
	0.41	0.56:	4.9	15.3	PS				
NGC 4651	0.54	0.60	6.5	15.8	AS	33.4	350	68.2	2.9
	0.40	0.41	5.2	15.1	PS				
NGC 4654	1.65	1.35	14.3	34.9	AS	33.4	730	59.3	2.8
	0.86	1.32	13.0	34.4	PS				
NGC 4656/57	0.15	0.37	7.0	7.8	SV	46.9	...	314.4	...
	< 0.69	< 0.34	2.2	6.1	PS				

TABLE 3—*Continued*

Name	S_{12} (Jy)	S_{25} (Jy)	S_{60} (Jy)	S_{100} (Jy)	Source	T_d (K)	S_{CO} (Jy km s^{-1})	S_{HI} (Jy km s^{-1})	$F_{H\alpha}$ (10^{-12} ergs cm^{-2} s^{-1})
NGC 4666	3.46	3.47	36.3	77.7	AS	35.3	...	...	5.2
	1.09	1.64	25.5	75.9	PS				
NGC 4689	0.61	0.54	2.9	9.4	AS	30.5	710	8.3	1.4
	< 0.47	< 0.45	2.6	9.7	PS				
NGC 4698	< 0.08	< 0.06	0.3	1.9	AS	25.2	< 90	26.2	...
	< 0.25	< 0.31	< 0.5	1.8	PS				
NGC 4710	0.26	0.56	5.9	12.7	AS	34.9	200	< 0.6	...
	< 0.31	< 0.50	5.9	12.9	PS				
NGC 4713	0.33	0.20	4.4	10.9	AS	33.2	< 70	61.5	3.0
	< 0.32	< 0.54	4.4	10.2	PS				
NGC 4725	0.92	0.68	4.6	18.2	SV	28.6	...	88.3	...
	< 0.59	< 0.25	0.8	< 7.0	PS				
NGC 4736	5.75	5.90	75.2	111.1	AS	40.9	1830	65.9	14.1
	2.79	3.50	55.7	103.8	PS				
NGC 4746	0.48	0.62	4.7	12.6	AS	32.4	...	...	...
	0.43	0.52	4.6	11.6	PS				
NGC 4808	0.70	0.66	6.6	15.3	AS	34.0	<100	69.8	2.3
	0.68	0.70	6.7	14.7	PS				
Mrk 231	2.05	7.97	35.0	28.9	AS	55.1	85	<1.5	...
	1.82	8.56	33.3	30.0	PS				
NGC 4900	0.52	0.56	6.1	12.4	AS	35.9	...	20.0	3.0
	0.34	0.47	5.4	11.9	PS				
NGC 5033	1.95	2.37	21.6	51.0	SV	33.8	...	195.3	4.4:
	0.78	1.06	13.1	43.6	PS				
NGC 5055	5.77	6.76	50.9	155.2	SV	31.0	...	390.8	14.8:
	1.21	1.15	27.6	99.8	PS				
IC 883	0.30	1.28	14.9	25.0	AS	38.7	200	<1.5	...
	0.49	1.42	14.9	23.7	PS				
NGC 5194/95	11.98	15.89	130.3	284.9	SV	34.8	15200	216.5	30.2
	1.37	2.40	31.7	121.4	PS				
NGC 5236	26.67	41.31	291.9	538.4	SV	37.2	33100	1553.0	...
	4.72	19.61	103.2	212.0	PS				
NGC 5248	1.95	2.67	22.2	48.2	AS	34.9	...	94.3	4.7
	0.96	1.50:	17.5	43.0	PS				
NGC 5256	0.30	1.09	7.7	10.7	AS	42.0	180	...	...
	< 0.48	1.03	7.2	11.8	PS				
Mrk 273	0.24	2.18	23.5	22.2	AS	51.0	...	< 8.3	...
	< 0.31	2.34	23.4	21.6	PS				
NGC 5457	9.44	12.63	91.9	243.6	AO	32.5	...	2221.0	...
	< 0.52	0.35	3.8	29.9	PS				
NGC 5775	1.95	2.31	24.5	48.2	AS	36.4	...	46.3	...
	0.72	0.87	15.2	44.2	PS				
NGC 5866	0.35	0.32	4.9	16.4	AS	30.0	...	5.0	...
	0.38	0.24	5.1	16.5	PS				
NGC 5907	2.09	2.14	16.3	55.9	SV	30.0	...	206.3	...
	0.90	0.94	9.9	35.1	PS				
NGC 5936	0.64	1.46	9.4	17.1	AS	37.4	210	2.0	...
	0.48	1.29	8.8	16.1	PS				
Arp 220	0.60	8.03	111.9	110.9	AS	49.7	450	...	...
	0.48	8.15	103.7	116.2	PS				
NGC 6207	0.27	0.63	5.0	11.4	AS	34.2	75	34.6	2.6
	< 0.25	0.40	4.4	11.3	PS				
NGC 6240	0.73	3.50	23.5	27.0	AS	46.0	260	...	...
	0.57	0.52	23.2	25.9	PS				
NGC 6286	0.53	0.62	10.4	21.8	AS	35.4	250	...	...
	0.38	0.53	7.3	22.9	PS				
NGC 6384	0.54	0.48	5.0	14.4	SV	31.5	...	87.0	...
	< 0.25	< 0.25	1.8	12.8	PS				
NGC 6503	1.34	1.07	11.1	30.0	SV	32.3	960	154.6	4.9:
	0.75	0.50	7.1	24.7	PS				
NGC 6509	0.33	0.43	4.5	10.6	SV	33.9	...	...	...
	0.31:	0.34	3.2	7.2	PS				
NGC 6574	1.03	1.55	14.8	29.3	AS	36.2	550	5.0	1.6
	0.93	1.69	14.3	27.2	PS				
NGC 6643	1.35	1.27	12.1	32.2	AS	32.4	440	44.8	3.6
	0.67	0.98	10.1	31.0	PS				
NGC 6701	0.67	1.27	10.8	20.0	AS	37.2	280	...	...
	0.46	1.23	9.8	20.5	PS				

TABLE 3—*Continued*

Name	S_{12} (Jy)	S_{25} (Jy)	S_{60} (Jy)	S_{100} (Jy)	Source	T_d (K)	S_{CO} (Jy km s^{-1})	S_{HI} (Jy km s^{-1})	$F_{H\alpha}$ (10^{-12} ergs cm^{-2} s^{-1})
NGC 6921	0.56	0.93	10.1	14.8	AS	41.0	280	...	...
	0.58	1.07	11.0	17.1	PS				
NGC 6946	13.11	18.78	165.2	327.0	SV	36.3	8150	834.0	31.6
	2.17	6.56	52.1	126.4	PS				
NGC 7217	0.69	0.65	6.1	19.2	AS	30.7	440	12.6	2.1:
	0.47:	< 0.25	4.8	18.2	PS				
NGC 7331	4.32	4.70	41.9	114.2	SV	32.1	3460	201.6	...
	< 0.46	< 0.25	19.0:	80.9	PS				
NGC 7469	1.61	5.85	27.9	35.2	AS	43.9	310	3.2	...
	1.30	5.50	26.7	34.4	PS				
NGC 7479	1.49	3.60	15.1	24.3	AS	39.3	850	36.5	1.4:
	0.75	3.33	11.9	24.3	PS				
NGC 7541	1.58	1.99	21.2	39.4	AS	37.1	680	52.3	...
	0.92	1.57	18.3	39.0	PS				
NGC 7625	0.62	1.13	9.5	17.5	AS	37.3	190	17.4	...
	0.58	1.03	9.0	18.3	PS				
NGC 7674	0.72	1.83	5.2	7.7	AS	40.8	140	6.6	...
	0.72	1.93:	5.5	8.2	PS				
NGC 7741	0.43	0.28	2.9	6.8	SV	33.8	...	47.9	2.0
	<1.38	< 0.38	2.0	7.0	PS				
NGC 7771	0.93	2.11	21.6	36.8	AS	38.4	...	...	...
	0.68	1.73	17.9	37.9	PS				
IIZw 40	0.45	1.72	6.3	6.3	AS	49.1	21	17.6	...
	0.46	1.92	6.5	5.7:	PS				
IIZw 70	< 0.08	0.16	0.7	1.2	AS	38.4	<17	6.0	...
	...	...	...	...	PS				
IIIZw 102	0.62	1.13	9.5	17.5	AS	37.3	...	...	...
	0.58	1.03	9.0	18.3	PS				
DDO 47	0.08	< 0.10	0.1	0.4	AS	30.2	< 21	69.6	...
	...	...	...	...	PS				
DDO 050	< 0.09	0.13	0.8	2.2	AS	31.7	<17	284.6	...
	...	...	...	...	PS				
DDO 135	< 0.10	0.09	0.4	1.5	AS	30.1	< 25	18.3	...
	< 0.25	< 0.58	0.4:	1.3	PS				
DDO 155	0.18	0.18	0.2	< 0.4	AS	36.5	<12	8.4	...
	...	...	...	...	PS				
DDO 210	< 0.12	< 0.13	< 0.2	< 0.3	AS		13	12.7	...
	...	...	...	...	PS				
DDO 216	< 0.08	< 0.09	< 0.2	0.6	AS	< 29.1	13	22.4	...
	...	...	...	...	PS				
DDO 218	< 0.10	0.13	0.6	1.2	AS	36.1	81	13.8	...
	< 0.25	< 0.59	0.5:	1.1:	PS				
LGS 003	< 0.10	< 0.09	< 0.2	< 0.5	AS		26	1.4	...
	...	...	...	...	PS				
M81DwA	0.06	< 0.04	< 0.1	0.3	AS	< 31.5	<12	3.8	...
	...	...	...	...	PS				
Mrk 331	0.54	2.40	18.8	20.2	AS	47.6	430	7.0	...
	0.53	2.44	16.7	20.4	PS				

NOTES.—The columns are as follows:

Col. (1).—Galaxy name.

Cols. (2)–(5).—*IRAS* flux densities at 12, 25, 60, and 100 μm. Line 1 for each galaxy gives the best estimate of each flux density from co-added *IRAS* data, while line 2 gives the entries from the PSC.

Col. (6).—Source of *IRAS* data: AS = Addscan, SC = Survey Co-add, AO = Additional Observations. The uncertainties in the flux densities are typically ~10% for the addscans and ~20% for the SCs and AOs.

Col. (7).—Dust temperature computed from the ratio of 60 to 100 μm flux densities, a λ^{-1} emissivity law, and assuming a single temperature component.

Col. (8).—CO flux of the model distribution which best matches the observed distribution of integrated intensities when sampled with a 45″ Gaussian. Models are truncated at radius of outer edge of the telescope beam for the outermost CO observation. Corrections for source-beam coupling are applied. Uncertainties arising from incomplete sampling of the disk of a galaxy are typically ~20%, although this depends on the distance of the galaxy, the fraction of the disk sampled, and the shape of the CO distribution. The CO observations which were modeled are for 124 galaxies from published CO observations made at FCRAO (Young and Scoville 1982*a*, *b*, *c*; Scoville and Young 1983; Young, Tacconi, and Scoville 1983; Scoville, Young, and Lucy 1983; Young and Scoville 1984; Scoville *et al.* 1985; Young *et al.* 1986*a*, *b*; Sanders *et al.* 1986; Tacconi and Young 1987; Kenney and Young 1988*b*). The most uncertain flux values are those based on only one observation per galaxy (cf. Tacconi and Young 1987; Sanders *et al.* 1986). Even if all of the gas in a galaxy is sampled, the uncertainty in how that gas is distributed can lead to a 30% uncertainty in flux.

Col. (9).—H I flux from Huchtmeier *et al.* (1983). When several entries were found, an average was made of all those which covered the galaxy.

Col. (10).—Hα flux from Kennicutt and Kent (1983), Bushouse (1986), Kennicutt *et al.* (1987). The fluxes from Young, Kleinmann, and Allen (1988) are marked by the letter a; these have been corrected for extinction internal to the galaxy based on near-infrared emission-line imaging.

Columns (2)–(5).—Total flux densities at 12, 25, 60, and 100 μm (line 1), scaled by the appropriate values given in Table 2. For comparison, the PSC entries are also given at each wavelength (line 2).

Column (6).—The source of the flux densities for each galaxy (line 1), from either the Addscan (AS), Survey Co-add (SC), or Additional Observation (AO) results. In general, the Addscan flux densities were preferred over the SC flux densities because of the lower uncertainties, provided the source was not so extended that Addscan missed some of the flux (i.e., the source extent was less than the cross-scan width of the *IRAS* detectors, or $\sim 5'$). The PSC designation is given on line 2.

Column (7).—The dust temperature for each galaxy, T_D, derived from the S_{60}/S_{100} flux density ratio, assuming a single temperature component and λ^{-1} emissivity law.

Column (8).—The CO flux, in units of Jy km s^{-1}, derived from CO observations along the major axis of each galaxy and computed according to the method described in Kenney and Young (1988*b*). The CO flux listed is that belonging to the model distribution which best matches the observed CO integrated intensities when sampled with a 45″ Gaussian beam. These fluxes have been corrected for source-beam coupling. The CO fluxes listed have all been derived in a consistent manner for 124 galaxies from published CO observations made at FCRAO (Young and Scoville 1982*a*, *b*, *c*; Scoville and Young 1983; Young, Tacconi, and Scoville 1983; Scoville, Young, and Lucy 1983; Young and Scoville 1984; Scoville *et al.* 1985; Young *et al.* 1986*a*, *b*; Sanders *et al.* 1986; Tacconi and Young 1987; Kenney and Young 1988*b*). The uncertainties in the CO fluxes are generally $\sim$ 20%–30% depending on the fraction of the galaxy surface area which was sampled. The most uncertain fluxes are those based on only one observation per galaxy (cf. Sanders *et al.* 1986; Tacconi and Young 1987) since no constraints could be placed on the source distribution.

CO fluxes for 26 of these galaxies have been derived by Verter (1987). The biggest difference between the two methods of flux derivation is that Verter integrated her model distributions out to two-thirds of the optical radius (R_{25}), while we truncated each model distribution at the radius of the outer edge of the beam for the outermost CO observation. Because few galaxies have CO emission detected at radii as large as two-thirds R_{25}, Verter's extrapolations may include more emission than detected. This is likely, since for the 26 galaxies in common to the two studies, the CO fluxes in Verter (1987) are on average 2 times higher than those presented in Table 3. A more complete discussion of the CO properties of these and 100 additional galaxies observed in the FCRAO Extragalactic CO Survey will be presented elsewhere (Young *et al.* 1989).

Column (9).—The H I flux in units of Jy km s^{-1} from the catalog of Huchtmeier *et al.* (1983) and Warmels (1986). When multiple entries were found in Huchtmeier *et al.*, an average was taken for all those which covered the entire galaxy.

Column (10).—The Hα flux in units of 10^{-12} ergs cm^{-2} s^{-1} from Kennicutt and Kent (1983), Bushouse (1986), Kennicutt *et al.* (1987), and Young, Kleinmann, and Allen (1988). The Hα fluxes of Young, Kleinmann, and Allen (1988) have been corrected for extinction internal to the galaxy.

IV. RESULTS

a) Infrared Luminosities and Dust Masses

We have calculated the IR luminosities from $\sim$1 to 500 μm using both the 60 and 100 μm flux densities following the method described in the Appendix of *Cataloged Galaxies in the IRAS Survey* (1985). Assuming a single temperature component and a λ^{-1} emissivity law, the IR luminosity ($L_{\rm IR}$) is given by

$$L_{\rm IR} = 4\pi D^2\left[1.26C\left(2.58\times10^{-14}S_{60} + 1.0\times10^{-14}S_{100}\right)\right]. \quad (1)$$

Here, D is the distance, the factor 1.26 corrects for the gap between the 60 and 100 μm bandpasses, and the filter response as a function of λ; S_{60} and S_{100} are the flux density at 60 and 100 μm in Jy; the constant C corrects for the flux missed beyond 120 μm and shortward of 40 μm and is a function of the S_{60}/S_{100} ratio. In terms of solar units, equation (1) becomes

$$L_{\rm IR} = 3.75\times10^5 D^2 C(2.58 S_{60} + S_{100}), \quad (2)$$

where D is in Mpc, S_{60} and S_{100} are in Jy, and the values of C are given in Table B.1 of *Cataloged Galaxies in the IRAS Survey* (1985). The computed values of $L_{\rm IR}$ are listed in Table 4.

We have also used the infrared flux densities to estimate the mass of warm dust in each galaxy. Following the analysis of Hildebrand (1983) and assuming a single temperature component, the mass of warm dust ($M_{\rm dust}$) is given by

$$M_{\rm dust} = (4/3)\,a\rho/Q_\nu\left[S_\nu D^2/B(\nu,T)\right], \quad (3)$$

where a is the weighted grain size, ρ is the grain density, Q_ν is the grain emissivity, S_ν is the flux density at wavelength ν, and $B(\nu,T)$ is the intensity of the blackbody of temperature T at wavelength ν. Using the values of grain size, grain density, and emissivity given by Hildebrand (1983), the quantity $(4/3)a\rho/Q_{100} = 0.04$ g cm^{-2}. For the 100 μm–emitting dust, equation (3) then becomes

$$M_{\rm dust} = 4.78 S_{100} D^2\left[\exp\left(143.88/T_{\rm dust}\right) - 1\right], \quad (4)$$

where the dust mass is in $M_\odot$, S_{100} is in Jy, D is in Mpc, and the dust temperature is in K. As discussed in Young *et al.* (1986*b*), *IRAS* is sensitive to warm dust with $T \gtrsim 25$ K, but not to cold dust with $T \gtrsim 20$ K emitting predominantly at wavelengths beyond 100 μm. Thus, we shall refer to the dust mass calculated using equation (4) as the "warm dust mass."

b) Global Galaxy Properties

In addition to the IR luminosities and dust masses for the galaxies in our sample, we have compiled information on the global galaxy properties from the literature. The entries in Table 4 are as follows:

Column (1).—Galaxy NGC, UGC, IC, Mrk, or DDO designation.

Column (2).—Distance computed from $V_{\rm LG}$ in Table 1 and assuming $H_0 = 50$ km s^{-1} Mpc^{-1}.

TABLE 4

Global Properties

Name	D (Mpc)	log L_{IR} ($L_\odot$)	log L_B ($L_\odot$)	log M_D ($M_\odot$)	log M_{HI} ($M_\odot$)	log M_{H2} ($M_\odot$)	L_{IR}/M_{H2} ($L_\odot/M_\odot$)	L_{IR}/L_B	Equivalent Width of Hα (Å)
NGC 7814	25.0	9.60	10.67	6.32	9.48	< 9.31	> 1.97	0.09	...
NGC 7817	28.5	10.14	10.02	6.75	9.45	9.46	4.78	1.30	...
NGC 23	95.9	11.28	11.22	7.39	10.29	10.35	8.57	1.14	...
NGC 157	35.0	10.79	11.01	7.23	10.36	...	...	0.60	28
NGC 185	0.7	5.87	8.08	2.78	5.62	...	...	0.01	...
NGC 205	0.7	6.31	8.51	3.47	4.41	...	...	0.01	...
NGC 253	3.3	10.42	10.27	6.54	9.65	9.37	11.24	1.42	...
NGC 278	17.7	10.25	10.30	6.40	9.38	...	...	0.88	36
NGC 520	45.4	11.12	10.89	7.22	10.10	10.40	5.19	1.71	...
NGC 628	15.9	10.29	10.80	6.87	10.50	...	...	0.30	24
NGC 660	19.6	10.79	9.85	6.75	10.23	...	...	8.67	...
NGC 695	198.4	11.86	11.43	8.07	< 10.45	10.99	7.48	2.71	...
NGC 828	112.2	11.57	11.30	7.90	10.40	10.80	5.94	1.86	...
NGC 834	94.6	11.14	11.14	7.48	10.07	10.18	9.25	1.01	...
NGC 864	32.7	10.10	10.75	6.53	10.38	9.54	3.62	0.23	...
NGC 877	82.3	11.29	11.18	7.58	10.68	10.39	7.88	1.29	...
NGC 891	14.1	10.62	10.56	7.14	9.93	10.01	4.08	1.16	...
NGC 972	33.4	10.93	10.63	7.14	9.62	...	...	2.02	...
NGC 992	84.9	11.22	10.81	7.23	10.34	...	...	2.58	...
NGC 1022	30.1	10.57	10.41	6.46	8.96	...	...	1.44	8
NGC 1055	21.5	10.49	10.54	7.00	10.00	10.42	7.89	0.89	...
NGC 1068	22.7	11.32	11.24	7.13	9.80	...	...	1.22	50
NGC 1084	28.1	10.73	10.80	7.00	10.05	...	...	0.86	41
NGC 1097	24.5	10.89	11.01	7.31	10.29	...	...	0.76	...
NGC 1156	9.7	9.12	9.47	5.27	9.23	...	...	0.44	99
NGC 1275	107.2	11.22	11.67	6.76	...	...	...	0.35	...
IC 342	4.6	10.17	10.37	6.60	10.28	9.75	2.60	0.62	...
UGC 2982	105.8	11.37	10.30	7.70	...	...	...	11.74	...
NGC 1530	53.3	10.90	10.65	7.40	10.36	10.15	5.73	1.81	...
NGC 1569	4.7	9.40	9.30	4.88	8.69	6.94	285.50	1.24	149
NGC 1614	92.9	11.76	10.87	7.43	9.88	10.41	22.40	7.75	164
NGC 1620	68.7	10.46	10.74	7.08	10.40	...	...	0.52	...
NGC 2146	20.6	11.10	10.61	6.99	10.10	10.09	10.36	3.10	...
NGC 2339	46.7	10.97	10.91	7.11	10.05	10.32	4.46	1.13	...
NGC 2276	51.6	10.96	11.04	7.33	10.10	10.36	4.01	0.83	42
NGC 2403	3.3	9.22	9.91	5.62	9.62	7.83	25.02	0.21	...
NGC 2532	104.2	11.13	11.18	7.64	10.52	10.15	9.59	0.89	...
NGC 2623	107.1	11.76	10.64	7.41	9.58	10.37	25.05	13.34	5.8
NGC 2633	46.0	10.85	10.58	7.01	10.01	9.88	9.33	1.87	...
NGC 2681	15.2	9.54	10.24	5.72	...	...	...	0.20	< 4
NGC 2775	19.3	9.61	10.42	6.44	8.76	9.35	1.81	0.15	< 2
Arp 55	239.4	11.88	11.10	7.92	...	11.06	6.50	5.98	...
NGC 2798/99	34.2	10.69	10.29	6.73	9.45	8.67	106.92	2.55	...
NGC 2841	14.0	9.71	10.65	6.54	9.80	9.66	1.12	0.11	< 4
NGC 2903	9.3	10.12	10.51	6.34	9.63	...	...	0.41	...
NGC 3034	3.3	10.50	9.74	6.13	9.14	9.21	19.40	5.74	56
NGC 3079	24.2	10.86	10.79	7.13	10.17	10.21	4.45	1.17	...
NGC 3077	3.3	8.58	9.12	4.68	8.88	...	...	0.29	...
NGC 3156	19.1	8.44	9.76	5.23	8.07	...	...	0.05	...
NGC 3147	57.6	11.01	11.28	7.76	10.12	10.70	2.07	0.53	...
NGC 3184	11.9	9.68	10.27	6.33	9.63	...	...	0.26	...
NGC 3221	77.5	11.11	10.51	7.60	10.41	10.29	6.60	3.98	...
Mrk 33	30.4	9.92	9.86	5.86	9.04	...	...	1.14	...
NGC 3310	21.3	10.51	10.49	6.37	9.93	8.86	44.92	1.05	113
NGC 3344	10.3	9.50	10.11	6.07	9.62	8.89	4.05	0.25	...
Mrk 35	19.0	9.60	9.61	5.47	8.99	8.00	39.67	0.98	...
NGC 3368	15.5	9.87	10.66	6.38	9.57	...	...	0.16	5
NGC 3437	20.8	10.04	10.00	6.22	9.63	8.96	11.98	1.09	...
NGC 3504	29.6	10.62	10.53	6.70	8.97	9.55	11.97	1.25	35
NGC 3521	12.8	10.36	10.70	6.84	10.00	9.95	2.60	0.46	14
NGC 3556	15.4	10.36	10.57	6.77	9.95	9.42	8.58	0.62	...
NGC 3623	6.7	8.92	10.01	5.74	8.20	< 8.53	> 2.49	0.08	< 2
NGC 3627	6.7	9.88	10.14	6.29	8.63	9.24	4.37	0.54	18
NGC 3628	6.7	9.80	10.06	6.19	9.45	9.20	4.00	0.55	...
NGC 3690	62.1	11.99	...	7.49	< 9.73	10.34	45.13	...	...

TABLE 4—*Continued*

Name	D (Mpc)	$\log L_{IR}$ ($L_{\odot}$)	$\log L_B$ ($L_{\odot}$)	$\log M_D$ ($M_{\odot}$)	$\log M_{HI}$ ($M_{\odot}$)	$\log M_{H2}$ ($M_{\odot}$)	L_{IR}/M_{H2} ($L_{\odot}/M_{\odot}$)	L_{IR}/L_B	Equivalent Width of Hα (Å)
NGC 3893	20.7	10.26	10.53	6.71	9.89	9.40	7.08	0.53	...
NGC 3992	23.0	10.01	10.83	6.91	10.01	...	...	0.15	...
NGC 4030	25.1	10.53	10.16	7.07	10.00	...	...	2.37	...
NGC 4038/39	28.9	10.91	10.76	7.14	9.99	10.09	6.60	1.41	...
NGC 4064	20.0	9.54	10.11	5.89	< 8.40	8.61	8.39	0.27	...
NGC 4088	16.4	10.26	10.38	6.62	9.84	...	...	0.75	...
NGC 4102	19.7	10.60	10.02	6.61	9.02	...	...	3.80	...
NGC 4192	20.0	10.00	10.68	6.57	9.93	9.62	2.40	0.21	...
NGC 4194	52.6	11.15	10.61	6.76	9.56	9.66	31.14	3.44	.
NGC 4212	20.0	9.87	10.18	6.28	< 8.45	9.35	3.30	0.49	20
NGC 4216	20.0	9.78	10.69	6.61	9.54	9.44	2.22	0.12	...
NGC 4236	3.2	8.08	9.47	4.32	9.15	...	...	0.04	...
NGC 4254	20.0	10.62	10.72	7.05	9.99	10.12	3.16	0.79	32
NGC 4258	10.7	10.00	10.87	6.62	10.09	...	...	0.13	...
NGC 4274	14.3	9.52	10.23	6.25	8.65	...	...	0.19	< 8
NGC 4273	20.0	10.01	10.01	6.43	9.22	...	...	0.99	...
NGC 4293	20.0	9.68	10.49	6.09	...	9.07	4.06	0.16	< 4
NGC 4294	20.0	9.45	9.95	5.73	9.47	< 8.42	> 10.60	0.31	55
NGC 4298/302	20.0	10.11	10.11	6.89	9.09	9.46	4.40	0.98	11
NGC 4299	20.0	9.36	9.73	5.71	9.15	...	...	0.43	71
NGC 4303	20.0	10.59	10.81	6.93	9.98	10.00	3.86	0.61	34
NGC 4312	20.0	9.46	9.89	6.14	...	8.85	4.09	0.37	...
NGC 4321	20.0	10.47	10.85	6.99	9.66	10.17	2.03	0.42	18
NGC 4380	20.0	9.10	9.59	6.01	8.35	< 8.42	> 4.82	0.33	...
NGC 4383	20.0	9.86	10.03	5.89	...	...	...	0.67	...
NGC 4388	20.0	9.98	10.33	6.15	8.93	9.01	9.36	0.45	...
NGC 4394	20.0	9.27	10.19	6.11	8.82	9.09	1.52	0.12	< 6
NGC 4402	20.0	9.85	9.59	6.57	8.83	9.44	2.56	1.84	...
NGC 4414	14.4	10.23	10.28	6.68	9.50	...	...	0.90	...
NGC 4418	38.2	1106	9.81	6.41	...	...	...	17.84	...
NGC 4419	20.0	9.88	10.37	6.24	8.22	9.61	1.86	0.32	...
NGC 4424	20.0	9.46	10.06	5.77	8.49	8.39	11.81	0.25	...
NGC 4438	20.0	9.68	10.64	6.28	8.86	8.97	5.13	0.11	...
NGC 4449	5.2	9.37	9.82	5.62	9.70	7.65	51.98	0.35	63
NGC 4450	20.0	9.52	10.55	6.36	8.55	9.30	1.66	0.09	...
NGC 4490/85	12.6	10.23	10.48	6.37	10.14	8.70	34.46	0.56	...
NGC 4486	20.0	8.51	11.05	4.13	10.31	...	...	0.003	< 6
NGC 4501	20.0	10.43	10.85	7.08	9.51	9.99	2.77	0.38	6
NGC 4526	20.0	9.83	10.72	6.33	...	< 8.60	> 16.93	0.13	< 4
NGC 4527	20.0	10.51	10.50	6.73	9.95	9.90	4.09	1.02	...
NGC 4532	20.0	9.90	10.09	6.14	9.66	< 8.42	> 29.84	0.64	...
NGC 4535	20.0	10.13	10.65	6.60	10.01	9.84	1.94	0.30	14
NGC 4536	20.0	10.43	10.59	6.36	9.83	9.51	8.23	0.68	18
NGC 4540	20.0	9.42	9.90	5.93	...	...	...	0.33	...
NGC 4548	20.0	9.64	10.51	6.56	9.28	9.38	1.83	0.13	3
NGC 4565	22.4	10.38	11.10	7.18	10.46	...	...	0.19	...
NGC 4567/68	20.0	10.42	10.09	6.99	9.31	9.66	5.64	2.10	14
NGC 4569	20.0	10.06	10.87	6.51	8.92	9.82	1.74	0.15	6
NGC 4571	20.0	9.42	9.45	6.28	9.09	9.22	1.57	0.94	10
NGC 4579	20.0	9.92	10.66	6.62	8.98	9.60	2.07	0.18	4
NGC 4594	19.3	9.94	11.27	6.77	8.97	...	...	0.05	2
NGC 4602	48.3	10.53	...	7.05	...	...	...	...	17
NGC 4605	5.7	9.08	9.54	5.41	8.60	7.84	17.35	0.35	...
NGC 4631	12.8	10.54	10.79	6.84	10.47	...	...	0.56	39
NGC 4639	20.0	9.35	10.03	5.91	9.25	< 8.49	> 7.19	0.20	...
NGC 4647	20.0	9.86	10.14	6.48	8.93	9.42	2.76	0.53	...
NGC 4651	20.0	9.86	10.40	6.39	9.81	9.19	4.70	0.29	20
NGC 4654	20.0	10.20	10.49	6.73	9.75	9.51	4.96	0.51	17
NGC 4656/57	13.2	9.38	10.43	5.16	10.11	...	...	0.09	...
NGC 4666	27.9	10.85	10.70	7.27	...	...	...	1.43	31
NGC 4689	20.0	9.62	9.77	6.33	8.90	9.49	1.33	0.71	13
NGC 4698	20.0	8.96	10.40	6.10	9.39	< 8.60	> 2.31	0.04	...
NGC 4710	20.0	9.78	10.29	6.21	< 7.75	8.94	6.81	0.30	...
NGC 4713	20.0	9.69	10.05	6.23	9.76	< 8.49	> 16.05	0.44	56
NGC 4725	22.6	10.01	11.04	6.87	10.03	...	...	0.09	...
NGC 4736	6.6	9.83	10.40	5.92	8.83	8.94	7.72	0.27	8
NGC 4746	20.0	9.76	9.73	6.34	...	...	...	1.06	...

TABLE 4—*Continued*

Name	D (Mpc)	$\log L_{IR}$ ($L_\odot$)	$\log L_B$ ($L_\odot$)	$\log M_D$ ($M_\odot$)	$\log M_{HI}$ ($M_\odot$)	$\log M_{H2}$ ($M_\odot$)	L_{IR}/M_{H2} ($L_\odot/M_\odot$)	L_{IR}/L_B	Equivalent Width of Hα (Å)
NGC 4808	20.0	9.85	9.98	6.34	9.82	< 8.64	> 16.08	0.74	43
Mrk 231	251.1	12.65	11.45	8.08	<10.35	10.77	75.57	15.89	...
NGC 4900	18.9	9.72	10.00	6.10	9.23	...	...	0.53	40
NGC 5033	19.2	10.34	10.69	6.83	10.23	...	...	0.45	17
NGC 5055	11.7	10.37	10.76	7.06	10.10	10.07	2.03	0.42	17
IC 883	138.8	11.80	10.69	8.00	< 9.83	10.63	15.02	13.03	...
NGC 5194/95	9.6	10.49	10.71	6.93	9.67	10.19	2.00	0.60	24
NGC 5236	8.9	10.73	10.95	7.02	10.46	10.46	1.86	0.60	...
NGC 5248	22.0	10.44	10.68	6.87	10.03	...	...	0.57	21
NGC 5256	167.4	11.64	11.10	7.67	...	10.75	7.73	3.45	...
Mrk 273	230.7	12.40	11.33	7.99	<11.02	...	...	11.86	...
NGC 5457	6.9	10.12	10.69	6.70	10.40	...	...	0.27	19
NGC 5775	31.6	10.77	10.60	7.11	10.04	...	...	1.50	...
NGC 5866	17.5	9.74	10.52	6.49	8.56	...	...	0.17	< 4
NGC 5907	15.6	10.18	10.55	6.93	10.07	...	...	0.43	...
NGC 5936	81.9	11.16	10.95	7.44	9.50	10.20	9.25	1.63	...
Arp 220	110.2	12.44	10.65	8.08	...	10.78	45.41	60.78	...
NGC 6207	21.3	9.78	10.20	6.25	9.57	8.57	16.08	0.38	35
NGC 6240	151.9	12.03	10.99	7.85	...	10.82	15.99	10.96	...
NGC 6286	116.8	11.55	10.78	7.95	...	10.57	9.44	5.87	...
NGC 6384	36.0	10.32	11.12	6.97	10.42	...	...	0.16	...
NGC 6503	6.3	9.13	9.73	5.73	9.16	8.62	3.20	0.25	19
NGC 6509	39.5	10.28	10.45	6.78	...	...	...	0.68	...
NGC 6574	50.2	10.95	10.81	7.30	9.47	10.18	5.93	1.38	27
NGC 6643	34.7	10.64	10.84	7.23	10.10	9.76	7.57	0.63	33
NGC 6701	84.5	11.26	11.09	7.54	...	10.34	8.31	1.45	...
NGC 6921	91.8	11.25	10.87	7.33	...	10.42	6.68	2.35	...
NGC 6946	10.1	10.61	10.80	6.96	10.30	9.96	4.45	0.64	29
NGC 7217	24.5	10.10	10.77	6.81	9.25	9.46	4.42	0.21	6
NGC 7331	22.1	10.80	11.08	7.40	10.37	10.27	3.40	0.53	...
NGC 7469	102.0	11.76	11.35	7.69	9.90	10.55	16.09	2.59	...
NGC 7479	52.1	10.95	11.09	7.12	10.37	10.40	3.51	0.72	12
NGC 7541	57.2	11.21	10.97	7.50	10.61	10.39	6.60	1.75	...
NGC 7625	37.3	10.49	10.35	6.77	9.76	9.45	10.80	1.38	...
NGC 7674	180.9	11.55	11.38	7.64	10.71	10.71	6.82	1.47	...
NGC 7741	20.4	9.51	10.20	6.01	9.67	...	...	0.20	24
NGC 7771	90.2	11.59	11.10	7.81	...	...	...	3.13	...
IIZw 40	13.8	9.38	8.23	5.05	8.90	7.64	54.03	13.94	...
IIZw 70	25.2	9.00	9.31	5.22	8.95	< 8.07	> 8.47	0.49	...
IIIZw 102	37.3	10.49	10.35	6.77	...	...	...	1.38	...
DDO 47	4.3	6.94	8.22	3.68	8.48	< 6.63	> 2.05	0.05	...
DDO 50	3.3	7.42	8.93	4.06	8.86	< 6.31	>13.01	0.03	...
DDO 135	20.0	8.81	9.10	5.56	9.24	< 8.04	> 5.93	0.52	...
DDO 155	2.3	< 6.40	7.13	< 2.74	7.02	< 5.84	...	< 0.19	...
DDO 210	1.5	< 5.93	6.41	< 2.26	6.83	5.51	< 2.67	< 0.34	...
DDO 216	1.6	< 6.20	7.84	3.02	7.13	5.56	< 4.29	< 0.02	...
DDO 218	31.6	9.16	9.69	5.52	9.51	8.95	1.62	0.30	...
LGS 003	0.8	< 5.56	5.79	< 2.33	5.32	5.26	< 2.00	< 0.59	...
M8 1DwA	3.3	< 6.50	6.59	3.15	6.99	< 6.16	...	< 0.82	...
Mrk 0331	112.2	11.67	...	7.42	10.32	10.78	7.83	...	...

Column (3).—Logarithm (base 10) of the infrared luminosity in $L_\odot$ from 1 to 500 μm, computed using equation (2). These luminosities are slightly smaller than those reported for 26 galaxies (Young *et al.* 1986*a*) because we have now scaled down the Addscan flux densities by ~10% (see Table 2).

Column (4).—Logarithm of the blue luminosity in $L_\odot$, computed from values of B_{T^0} in Table 1 and the distance, and assuming $M_{B_\odot} = +5.48$.

Column (5).—Logarithm of the warm dust mass in $M_\odot$, calculated using equation (4) along with the dust temperature and 100 μm flux density from Table 3.

Column (6).—Logarithm of the H I mass in $M_\odot$ from the H I fluxes in Table 3. The H I mass is given by

$$M_{HI} = 2.36 \times 10^5 D^2 S_{HI}, \quad (5)$$

where D is in Mpc and the H I flux, S_{HI}, is in Jy km s^{-1}. For galaxies which exhibit H I absorption, the derived H I masses are lower limits.

Column (7).—Logarithm of the H_2 mass in $M_\odot$ from the CO flux in Table 3, adopting a constant conversion from CO integrated intensities to H_2 surface densities of 2.8×10^{20} H_2

cm^{-2}/[K(T_R) km s^{-1}] (Bloemen *et al.* 1986). For this value of the $N(H_2)/I_{CO}$ conversion factor, Kenney and Young (1989) show that the H_2 mass in $M_\odot$ is given by

$$M(H_2) = 1.1 \times 10^4 D^2 S_{CO}, \tag{6}$$

where D is the distance in Mpc and the flux is in Jy km s^{-1}. Dickman, Snell, and Schloerb (1986) and Young *et al.* (1986*b*) have shown that the molecular mass is related to the gas temperature (T_{gas}) and density ρ by $M(H_2) \propto L_{CO}(T_{gas})(\rho^{-0.5})$. Thus, the assumption that the CO luminosity traces the molecular mass is a valid assumption provided that $T_{gas}(\rho^{-0.5})$ remains constant. To the extent that molecular clouds with higher densities are found in regions with higher temperatures, these two effects will tend to cancel each other (Scoville and Sanders 1987).

Column (8).—Ratio of the global IR luminosity (col. [3]) to H_2 mass (col. [7]) in units of $L_\odot/M_\odot$.

Column (9).—Ratio of the IR luminosity (col. [3]) to blue luminosity (col. [4]).

Column (10).—Observed Hα + [N II] emission equivalent width in Å from Kennicutt and Kent (1983), Bushouse (1986), and Kennicutt *et al.* (1987).

V. DISCUSSION

Here we compare the global IR luminosities with H_2 masses, H I masses, dust masses, blue luminosities, and Hα luminosities. We have chosen first to compare absolute luminosities and masses, and then to compare ratios of the luminosities, masses, and fluxes. There is a need for both types of comparison in investigating global galaxy properties. The value in comparing the absolute luminosities (for example IR vs. blue luminosity) is in determining the slope of a correlation and the scatter as a function of luminosity. The value in investigating galaxy properties normalized, for example, by luminosity or mass is that effects of galaxy size are removed.

a) Comparisons with Infrared Luminosity

Figures 1*a*–1*d* illustrate the comparison of the IR luminosities with dust masses, H_2 masses, H I masses, and B luminosities for the galaxies listed in Table 4, where the points are coded by dust temperature. A good correlation is expected for the IR luminosity–dust mass comparison, since the two quantities are both derived from the 100 μm flux density through equations (2) and (4); we show this plot simply to illustrate the scatter found when comparing two closely related quantities. It is apparent from Figure 1*a* that most of the scatter arises as a result of the observed spread in dust temperature from galaxy to galaxy and the strong temperature dependence of the IR luminosity on dust temperature; for galaxies of a given dust mass, those with higher T_{dust} have higher luminosities.

Comparison of Figures 1*b* and 1*c* indicates that there is a significantly better correlation between IR luminosities and H_2 masses (correlation coefficient = 0.93) than between IR luminosities and H I masses (correlation coefficient = 0.81) as found previously for a small sample of galaxies (Young *et al.* 1986*b*). A similar result was found by Rengarajan and Iyengar (1988). The data in Figure 1*b* are fitted by

$$L_{IR} \propto M(H_2)^{0.98 \pm 0.03}. \tag{7}$$

In determining the uncertainty in the exponent, upper limits were treated as having the 3 σ value. While some of the scatter in the L_{IR}–dust mass and $L_{IR}-M(H_2)$ comparisons is related to temperature (see Figs. 1*a* and 1*b*), this is *not* true for the $L_{IR}-M$(H I) comparison. We conclude that *the IR emission is more closely tied to the molecular gas than to the total atomic gas content for this sample of galaxies.*

Figure 1*d* shows the comparison of IR and blue luminosities for the galaxies in the sample, where the temperature segregation is again apparent. The temperature dependence of the ratio L_{IR}/L_B has been pointed out previously (see de Jong *et al.* 1984; Iyengar, Rengarajan, and Verma 1985). Here, we show that the slope of the $L_{IR}-L_B$ comparison is not unity, a point we will return to in § V*b*, so that some of the observed scatter in the global L_{IR}/L_B ratios for a sample of galaxies with a range of luminosity will be due to the nonunity slope.

Since the IR luminosity arises from heated dust (Telesco and Harper 1980; Rieke *et al.* 1980), the gas mass which is the most important to compare with the global IR luminosity is the interstellar medium (ISM) mass located in the vicinity of the heating sources, i.e., within the optical disk. For Virgo spirals, the IR luminosity has been compared with the H_2 + H I mass within the optical disk (Kenney and Young 1988*a*; see also discussion below.) Unfortunately, H I distributions with angular resolution $\leq 1'$ have been measured in only a fraction of the galaxies in our sample, so that this comparison for the entire sample must await additional observations.

It is important to consider that some of the IR emission in a galaxy may arise from dust heated by the ambient radiation field and not from newly formed stars. Lonsdale and Helou (1987) suggest that the far-IR emission in a galaxy consists of at least two components: a warm one which they associate with OB stars and star-forming complexes, and a cooler one which they attribute to dust in the neutral ISM (which they call "cirrus"-like) heated by the interstellar radiation field. One of the reasons they attribute the cool dust component to the neutral ISM is the known existence of cool cirrus emission associated with neutral material in the Galaxy (Low *et al.* 1984; Gautier 1986) and a cool component of dust observed in external galaxies (Telesco and Harper 1980; Smith 1982; Smith, Harper, and Lowenstein 1984). In their picture, galaxies with warm dust temperatures would be dominated by emission from star-forming regions, while emission from cool galaxies would be dominated by the "cirrus" component. However, the IR emission from giant molecular clouds in the Milky Way with H II regions has a low characteristic dust temperature when averaged over the cloud (T_{dust} = 29 K; Scoville and Good 1988), so that the molecular component could account for much of the cool emission in galaxies. In support of this suggestion, Figure 1*b* shows a good correlation between IR luminosities and molecular masses for *both* the galaxies with hot and cool dust temperatures; such a result is not expected if the model of Lonsdale and Helou (1987) is correct.

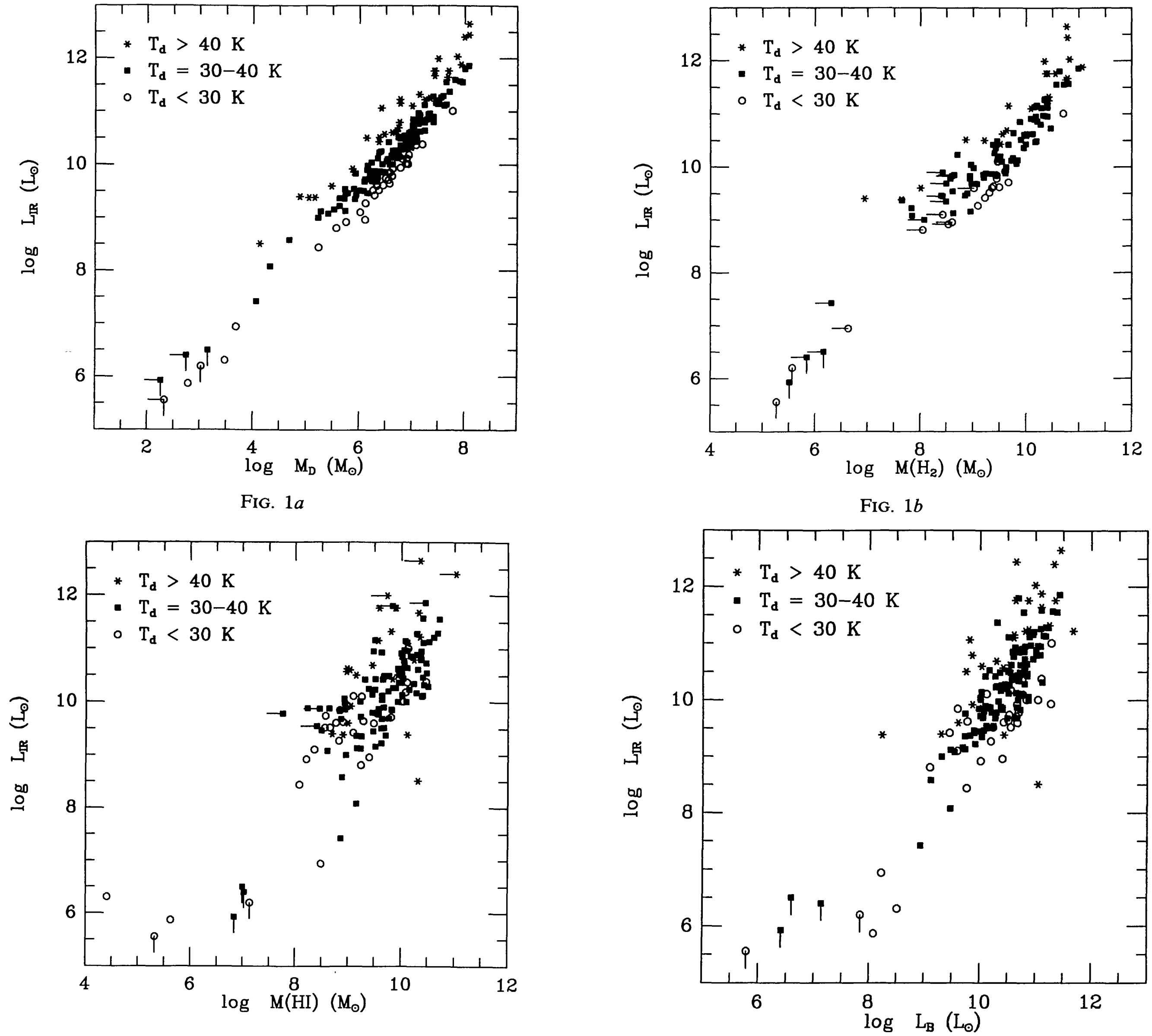

FIG. 1a

FIG. 1b

FIG. 1c

FIG. 1d

FIG. 1.—Comparison of IR luminosities with (*a*) dust masses, (*b*) H_2 masses, (*c*) H I masses, and (*d*) blue luminosities. Data points are coded by dust temperature to illustrate that some of the scatter observed is correlated with T_{dust}. Coding of the points is as follows: asterisks for $T_{dust} > 40$ K, squares for $T_{dust} = 30$–40 K, and circles for $T_{dust} < 30$ K.

In a recent investigation of M31 using *IRAS* observations, Walterbos (1987) concluded that the 60 and 100 μm emission arise predominantly from dust associated with atomic gas which is heated by the ambient interstellar radiation field. We point out here that the H_2 distribution in M31 derived from minor-axis CO observations (Stark 1979) is similar in shape and surface density to the azimuthally averaged H I distribution (Brinks 1984), making it difficult to distinguish the contributions to the IR luminosity from dust in atomic versus molecular clouds in M31.

While the *IRAS* observations of most galaxies do not provide sufficient spatial resolution to determine the distributions of 60 and 100 μm emission, the 170 μm observations of NGC 6946 and M51 (Smith 1982); Smith, Harper, and Lowenstein 1984) have been compared with both the CO and H I distributions in M51 and NGC 6946. Maloney (1987) concludes that the 170 μm flux cannot be produced by dust associated with atomic hydrogen, even allowing for the existence of radial variations in the metallicity and in the intensity of the interstellar radiation field. Furthermore, he concludes that the observed 170 μm emission can be produced by dust associated with the molecular gas. The apparent conflict between the conclusions of Maloney and Walterbos can easily be understood when it is realized that the H_2/H I ratios are very different for M31 relative to NGC 6946 and M51. In M31, the molecular and atomic gas mass surface densities are comparable (Stark 1979; Brinks 1984), while in NGC 6946 and M51 the molecular mass exceeds the atomic gas mass

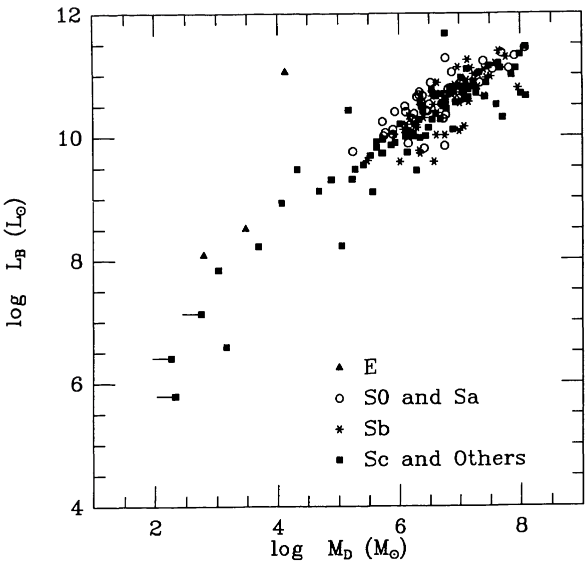

FIG. 2*a*

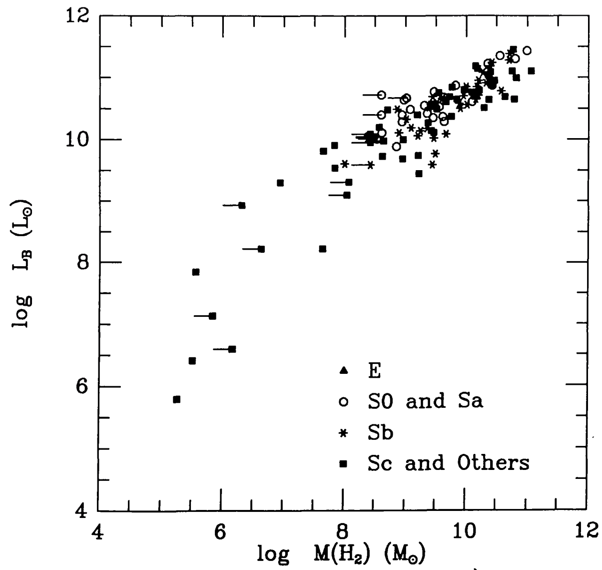

FIG. 2*b*

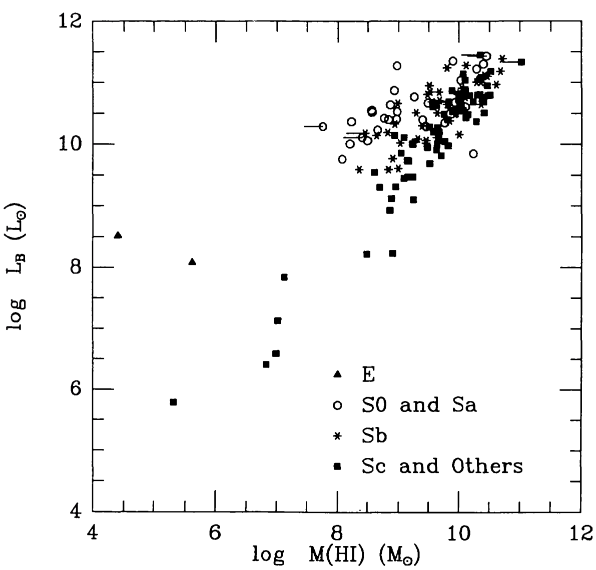

FIG. 2*c*

FIG. 2.—Comparison of blue luminosities with (*a*) dust masses, (*b*) H_2 masses, and (*c*) H I masses. Data points are coded by morphological type as follows: filled triangles for E, circles for SO and Sa, asterisks for Sb, and squares for Sc and others.

over the optical disk, with H_2/H I ratios of 100 near the centers (Young and Scoville 1982*a*; Scoville and Young (1983). Thus, the fraction of the IR emission which is contributed by dust in atomic clouds relative to dust in molecular clouds should depend on the H_2/H I ratio in a galaxy.

The H_2/H I ratio in galaxies is found to vary by more than a factor of 100 from the inner disk to the outer disk and from galaxy to galaxy (see Young and Scoville 1982*a*; Morris and Rickard 1982; Young *et al.* 1986*b*). Young and Scoville (1982*b*) have shown that the CO luminosities in the central 5 kpc of a small sample of Sc galaxies are proportional to the blue luminosities in the same regions over 2 orders of magnitude, while the central H I masses do not vary much from galaxy to galaxy within the sample. This indicates that the H_2/H I ratio is a function of luminosity in Sc galaxies, such that the more luminous galaxies have a higher fraction of their central gas mass in molecular form and the less luminous galaxies (e.g., M33 and NGC 2403) have a higher fraction of their central gas mass in atomic form.

The above arguments indicate that low-luminosity galaxies provide a sensitive test of the hypothesis that dust in both the atomic and molecular clouds contributes to the IR luminosity. A comparison of the IR luminosities and H_2 and H I masses has been carried out for an optically selected sample of 33 Virgo Sbc-Sm galaxies (Kenney and Young 1988*a*). For these 33 galaxies, the gas mass quantity which exhibits the best correlation with L_{IR} is the H_2 + H I mass *within the optical diameter* (i.e., the 25 mag arcsec^{-2} isophote). Among the Virgo galaxies with $L > 10^{10}$ $L_\odot$, the IR luminosity exhibits an excellent correlation with the H_2 mass. For luminosities less than 10^{10} $L_\odot$, Kenney and Young found that there is considerable scatter in that some galaxies are H_2 dominated while some are H I dominated. This scatter for the low-luminosity late-type Virgo spirals is decreased only by comparing the IR luminosity with the ISM mass within the optical disk; using the total H I mass does not improve the correlation since outer galaxy H I does not have much associated FIR emission (Walterbos 1987; Kenney and Young 1988*a*). This is a very reasonable result when one considers that the heating sources for the dust, whether sites of newly formed stars or older generations of stars, are more concentrated toward the center. Thus, the contribution to the IR luminosity from dust in H I clouds appears to become important in low-luminosity galaxies, where the ISM within the optical disk is primarily atomic. It is important to note that the low-luminosity Virgo galaxies studied by Kenney and Young have dust temperatures which range from 28 to 38 K; the galaxies which are H I dominated in the inner disk have the *same* mean dust temperature as the galaxies which are H_2

dominated. This result contradicts one of the underlying assumptions of Lonsdale and Helou (1987). Thus, the color temperature of a galaxy does not by itself allow one to distinguish between dust in atomic versus molecular clouds as the source of the IR emission or to distinguish between star formation versus the interstellar radiation field as the luminosity source. Clearly, as Kenney and Young have shown for the Virgo spirals with $L_{\mathrm{IR}} \gtrsim 10^{10}\ L_{\odot}$, the ISM mass within the optical disk is predominantly molecular, so that it must be the dust in the molecular clouds which produces most of the observed IR emission in these systems.

b) *Comparisons with Blue Luminosity*

Figures $2a-2c$ illustrate the comparisons of blue luminosity with dust mass, $\mathrm{H_2}$ mass, and H I mass. The greatest amount of scatter is found for the $L_B - M(\mathrm{H\ I})$ comparison (correlation coefficient = 0.79), while the best fit is found for the $L_B - M(\mathrm{H_2})$ comparison (correlation coefficient = 0.90), such that

$$L_B \propto M(\mathrm{H_2})^{0.72 \pm 0.03}. \tag{8}$$

The blue luminosity for the disk of a galaxy, ignoring the contribution from the bulge, is primarily from stars with ages less than several billion years (Searle, Sargent, and Bagnuolo 1973). It is noteworthy that the comparison of the global blue luminosities and $\mathrm{H_2}$ masses has a slope less than 1, while comparison of the blue luminosities and $\mathrm{H_2}$ masses *in the central* 5 *kpc* of nine galaxies yields a slope of 1 (Young and Scoville 1982*b*). This suggests that the blue light and $\mathrm{H_2}$ distributions in low- and high-luminosity galaxies are not homologous. The small extent of CO distributions in low-luminosity galaxies indicates that a considerable amount of blue light probably originates from outside of the region where the molecular gas is found. Such a trend will tend to decrease the slope of the global $L_B - M(\mathrm{H_2})$ comparison; another effect which could cause the shallow slope is extinction of the blue light in luminous galaxies, as discussed below. The simplest interpretation of the $L_B - M(\mathrm{H_2})$ correlation is that galaxies with more molecular gas have formed more stars integrated over the last several billion years.

The data in Figure 2 are coded by galaxy type, from which it is apparent that considerable scatter in L_B is observed for galaxies of a given $\mathrm{H_2}$ or H I mass and type. The most apparent difference among the galaxies is seen in the $L_B - M(\mathrm{H\ I})$ comparison (see Fig. 2*c*), where the early-type spirals of a given H I mass have higher luminosities than the late-type spirals; the result that $M(\mathrm{H\ I})/L_B$ increases with morphological type has been known for a number of years (see Roberts 1969; Shostak 1978). For the present sample, this result could be produced in part by the inclusion of early-type Virgo spirals, many of which are known to be deficient in atomic gas. Given the type dependence of $L_B/M(\mathrm{H\ I})$, it is interesting that the global values of $L_B/M(\mathrm{H_2})$ show no statistically significant type dependence.

The difference in the slopes of the fits to the $L_B - M(\mathrm{H_2})$ and $L_{\mathrm{IR}} - M(\mathrm{H_2})$ relations is significant. The smaller exponent in the $L_B - M(\mathrm{H_2})$ comparison (0.72 ± 0.03 from eq. [8]) relative to the $L_{\mathrm{IR}} - M(\mathrm{H_2})$ comparison (1.0 ± 0.03 from eq. [7]) may arise due to extinction of the blue light in galaxies with larger $\mathrm{H_2}$ masses, since these galaxies also have higher $\mathrm{H_2}$ surface densities and therefore larger dust column densities in their central regions. This conclusion also has implications for the well-known correlation of $B-H$ color with absolute magnitude or galaxy mass (e.g., Kraan-Korteweg, Cameron, and Tammann 1988), such that bigger galaxies are redder. While part of this trend is probably due to different star-formation histories of galaxies, an assertion which is supported by the correlation of galaxy mass with metallicity (see Pagel and Edmunds 1981), part of the correlation of $B-H$ color with galaxy mass could also be produced by extinction.

c) *Comparisons with Dust Masses*

Figures $3a-3d$ show the comparison of $\mathrm{H_2}$, H I, and total $\mathrm{H_2}$ + H I masses with dust masses. The best correlation found is for the $M(\mathrm{H_2}) - M_{\mathrm{dust}}$ comparison, with a correlation coefficient of 0.97, compared with 0.79 for the comparison of $M(\mathrm{H\ I})$ with M_{dust}. For the sample galaxies, we find

$$M(\mathrm{H_2}) \propto M_{\mathrm{dust}}^{1.04 \pm 0.02}. \tag{9}$$

The mean value for the observed $M(\mathrm{H_2})/M_{\mathrm{dust}}$ ratio is 570 ± 50, a value which is significantly different from the value of ~ 150 for the Milky Way (Draine and Lee 1984). Since *IRAS* is sensitive primarily to warm dust, the warm dust mass is an underestimate of the total dust mass for galaxies with a significant fraction of dust colder than ~ 30 K.

Figures $3a-3c$ are coded by galaxy type and illustrate that the different morphological types show similar values of the ratio $M_{\mathrm{gas}}/M_{\mathrm{dust}}$. The possibility that early-type galaxies have lower ratios of $M_{\mathrm{gas}}/M_{\mathrm{dust}}$ may reflect the fact that some dust is associated with evolved stars in the bulges of these galaxies, thus raising the dust mass and lowering the gas-to-dust ratio. Figure 3*d* shows the dust mass–$\mathrm{H_2}$ mass comparison from Figure 3*a*, but with the galaxies coded by dust temperature. This illustrates that there is no residual scatter that arises from the range of dust temperatures of the galaxies in the sample.

The fits to the data plotted in Figures 1–3 and the correlation coefficients for the fits are given in Table 5.

d) *Gas Depletion Time Scales*

In Figure 4 we show a plot of the total luminosity ($L_{\mathrm{IR}} + L_B$) versus the total interstellar gas mass $[M(\mathrm{H_2}) + M(\mathrm{H\ I})]$ for the program galaxies. Under the assumption that stars process 13% of their mass through the CNO cycle while on the main sequence (Schwarzschild 1958), the total luminosity of a galaxy can be related to the star formation rate (see eq. [13] of Scoville and Young 1983) by

$$\dot{M}_{\mathrm{O,B,A}} = 7.7 \times 10^{-11}\ L_{\mathrm{tot}}/L_{\odot}, \tag{10}$$

where $\dot{M}_{\mathrm{O,B,A}}$ is the rate at which mass is used to form O, B, and A stars ($M > 2\ M_{\odot}$; Tinsley 1980) in units of $M_{\odot}\ \mathrm{yr}^{-1}$. We note that this relation applies to galaxies whose luminosity is dominated by O, B, and A stars (i.e., it does not apply to

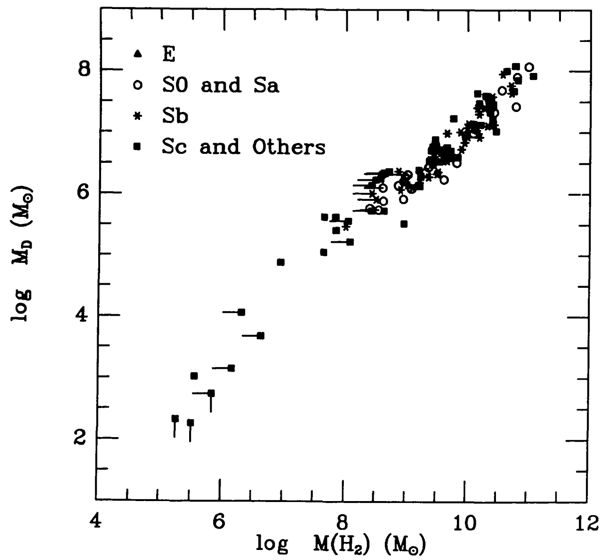

FIG. 3*a*

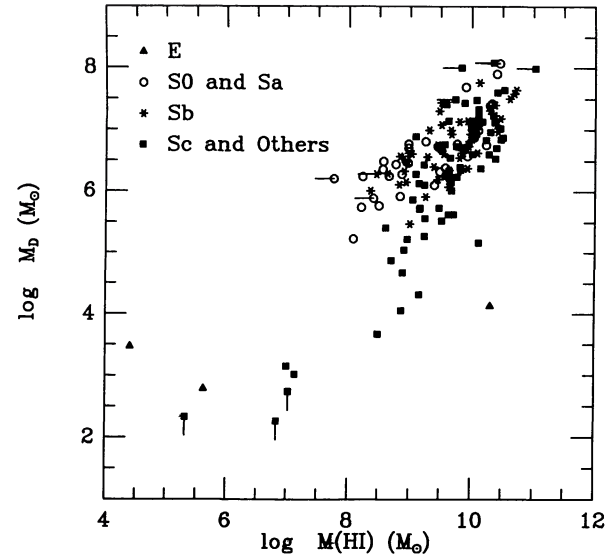

FIG. 3*b*

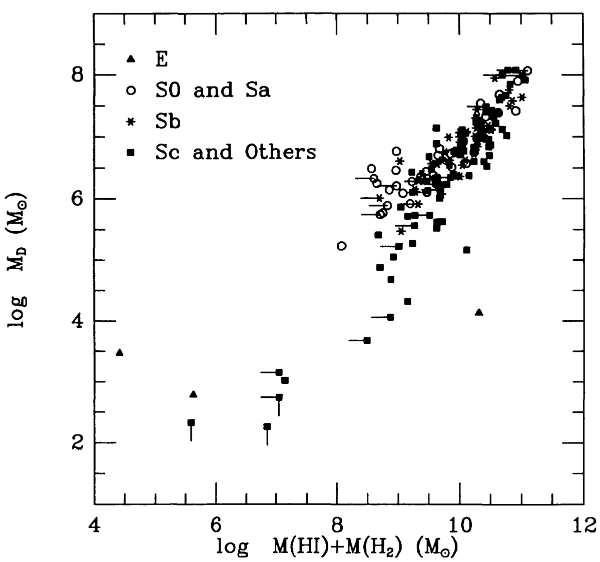

FIG. 3*c*

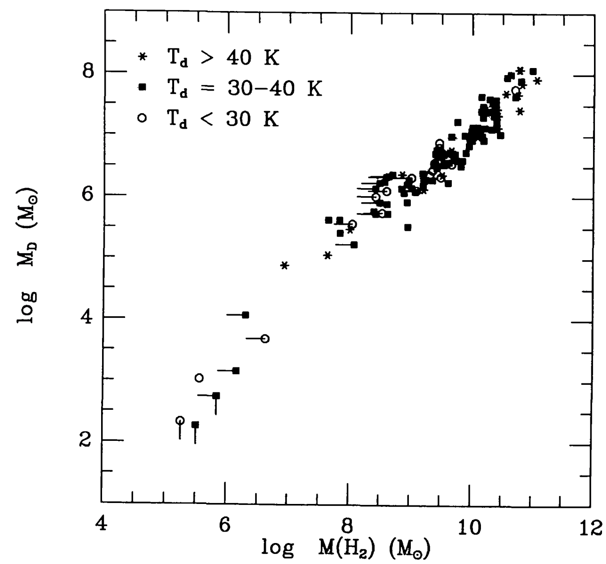

FIG. 3*d*

FIG. 3.—Comparison of dust masses with (*a*) global H_2 masses, (*b*) H I masses, and (*c*) with total H_2 + H I masses. Data points are coded by galaxy type as follows: filled triangles for E, circles for SO and Sa, asterisks for Sb, and squares for Sc and others. (d) The dust mass–H_2 mass comparison coded by temperature as in Fig. 1.

ellipticals). The majority of the galaxies plotted in Figure 4 have O, B, and A star formation rates between 0.01 and 100 $M_\odot$ yr^{-1}. If the present star formation rate in a galaxy is sustained, the global gas supply will be available for a time $\tau = M_{\rm gas}/\dot{M}_{\rm O,B,A}$, or between 10^8 and 10^{10} yr. Of course, small regions in some galaxies may use up gas in much less than 10^8 yr, while other regions may have depletion times longer than 10^{10} yr.

e) The Star Formation Efficiency in Galaxies

Figures 5*a*–5*c* illustrate the comparisons of the ratios $L_{\rm IR}/M(\rm H_2)$, $L_{\rm IR}/M$(H I), and $L_{\rm IR}/L_B$ versus the S_{60}/S_{100} ratio, or dust temperature. The $L_{\rm IR}/M$(H I) plot shows significant scatter, with no obvious trend. Both $L_{\rm IR}/M(\rm H_2)$ and $L_{\rm IR}/L_B$ are found to increase with dust temperature, which primarily reflects the high temperature dependence of the IR luminosity. The best correlation in Figure 5 is found for the ratio $L_{\rm IR}/M(\rm H_2)$ versus S_{60}/S_{100}, such that

$$L_{\rm IR}/M(\rm H_2) \propto T_{\rm dust}^{4.9\pm0.4}. \qquad (11)$$

Young *et al.* (1986*b*) use the correlation of $L_{\rm IR}/M(\rm H_2)$ versus S_{60}/S_{100} for a small number of galaxies to argue that the IR luminosity arises primarily from dust associated with molecular clouds, a conclusion which is strengthened by the larger statistics presented in Figure 5*a*.

TABLE 5

RESULTS OF FITS FOR LUMINOSITY AND MASS COMPARISONS

Quantities Plotted		Number of Galaxies	Fit: $y = ax^b$		Correlation Coefficient, r
y	x		a	b	
L_{IR}	M_D	182	1.7×10^3	1.06 ± 0.02	0.96
L_{IR}	$M(H_2)$	124	1.1×10^1	0.98 ± 0.03	0.93
L_{IR}	M(H I)	160	3.6×10^0	1.00 ± 0.06	0.81
L_{IR}	L_B	179	1.1×10^{-2}	1.17 ± 0.05	0.85
L_B	M_D	179	5.3×10^5	0.71 ± 0.03	0.88
L_B	$M(H_2)$	122	3.6×10^3	0.72 ± 0.03	0.91
L_B	M(H I)	158	2.2×10^3	0.73 ± 0.04	0.79
$M(H_2)$	M_D	124	4.0×10^2	1.04 ± 0.02	0.97
M(H I)	M_D	160	9.6×10^4	0.70 ± 0.04	0.79
M_{gas}	M_D	170	4.9×10^4	0.75 ± 0.04	0.87
$L_{IR}/M(H_2)$	T_D	124	2.2×10^{-7}	4.9 ± 0.4	0.74
L_{IR}/M(H I)	T_D	160	1.1×10^{-5}	3.6 ± 0.8	0.34
L_{IR}/L_B	T_D	179	6.6×10^{-10}	5.8 ± 0.6	0.62
L_{IR}	$L(H\alpha)$	49	3.0×10^2	1.02 ± 0.12	0.78
EWHα	$L_{IR}/M(H_2)$ for Sbc galaxies	26	11	0.52 ± 0.06	0.86

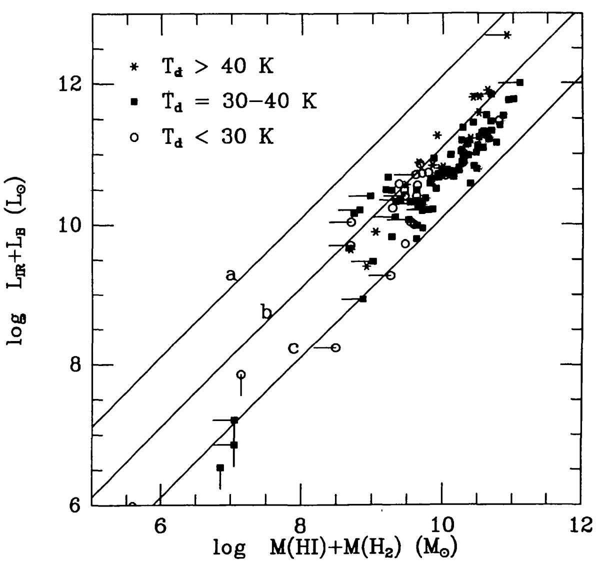

FIG. 4.—Comparison of total luminosity ($L_{IR} + L_B$) with total gas mass (H_2 + H I). The three lines illustrate gas depletion times of (a) 10^8, (b) 10^9, and (c) 10^{10} yr, given that the total luminosity indicates the star formation rate from eq. (10), and assuming that the star formation rate remains constant in time. Points are coded by dust temperature as indicated.

The exponent derived in equation (11) is straightforward to understand, since the IR luminosity depends on T^{4+n} for an emissivity law given by λ^{-n}, where $n = 1$ has been used in the present analysis. While the H_2 mass has a dependence on the mean gas temperature (Dickman, Snell, and Schloerb 1986; Young *et al.* 1986*b*; Scoville and Sanders 1987), we have derived H_2 masses assuming a single constant of proportionality between CO luminosity and H_2 mass. Thus, the temperature dependence expected for the $L_{IR}/M(H_2)$ ratio in Figure 5*a* is a T^5 dependence, as observed.

Considerable scatter is seen in the plot of L_{IR}/L_B versus S_{60}/S_{100} (Fig. 5*c*), although part of this is due to the fact that the slope of the $L_{IR}-L_B$ comparison is not 1 (see also Fig. 1*d*). That is, the L_{IR}/L_B ratio in galaxies is a function of IR luminosity such that higher ratios are found in more luminous galaxies. As suggested above (see § V*b*), this may result from greater extinction of the blue light in the more luminous galaxies.

If the IR luminosity is a measure of the star formation rate in a galaxy, the quantity $L_{IR}/M(H_2)$ provides a measure of the globally averaged star formation efficiency (SFE). While this is not a true efficiency in the sense that it measures the luminosity-to-mass ratio and is not dimensionless, the luminosity-to-mass ratio is the inverse of the gas depletion time scale if the present star formation rate is maintained. From galaxy to galaxy, we find that $L_{IR}/M(H_2)$ may have values ranging from a few $L_\odot/M_\odot$ to more than 100 $L_\odot/M_\odot$. As was shown for a smaller sample of galaxies (Young *et al.* 1986*a*; Solomon and Sage 1988), the lowest values of $L_{IR}/M(H_2)$ are found in isolated galaxies, and the highest values of $L_{IR}/M(H_2)$ are found in morphologically peculiar or merging and interacting galaxies.

As evidence that L_{IR} measures the SFR and that $L_{IR}/M(H_2)$ measures the SFE, we show in Figure 6*a* the comparison of the IR and Hα luminosities in 49 spiral and irregular galaxies which this study has in common with Kennicutt and Kent (1983), Bushouse (1986), and Kennicutt *et al.* (1987) and Young, Kleinmann, and Allen (1988). The IR and Hα luminosities are linearly related in this sample, such that

$$L_{IR} \propto L(H\alpha)^{1.0\pm0.1} \tag{12}$$

We note that the observed Hα luminosity of a galaxy may underestimate the ionizing star luminosity because of extinction of the Hα, except in the study of Young, Kleinmann, and Allen (1988) where extinction corrections were derived from near-infrared emission-line imaging. On the other hand, the IR luminosity may overestimate the SFR in a galaxy because of sources other than young stars which heat the dust. The

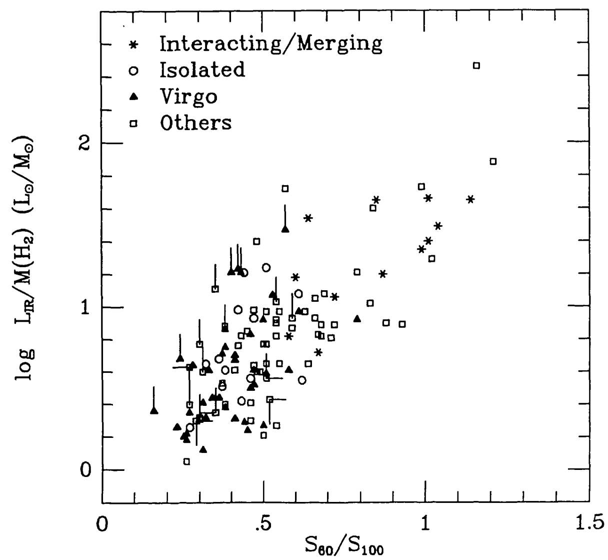

FIG. 5*a*

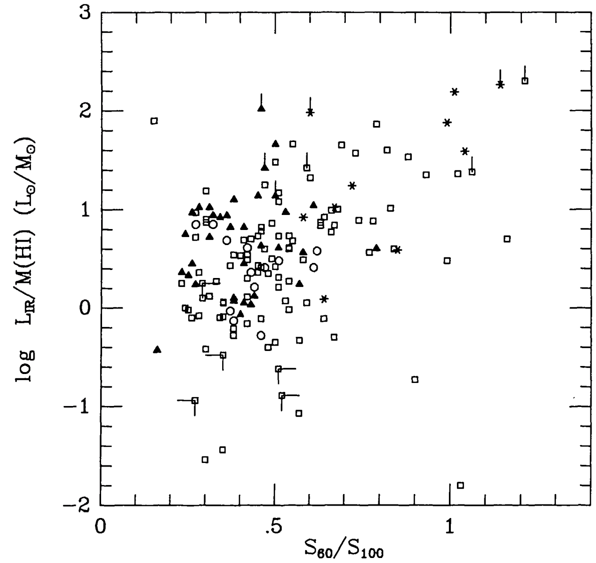

FIG. 5*b*

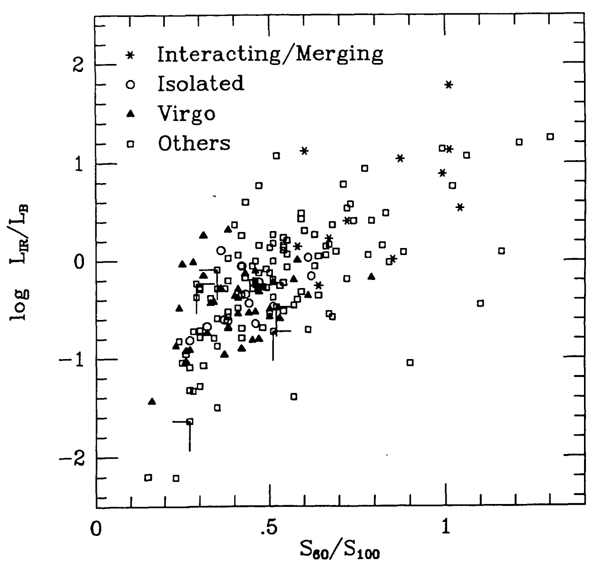

FIG. 5*c*

FIG. 5.—Comparison of the quantities (*a*) $L_{IR}/M(H_2)$ with S_{60}/S_{100}, (*b*) $L_{IR}/M(H\,I)$ with S_{60}/S_{100}, and (*c*) L_{IR}/L_B with S_{60}/S_{100}. Points are coded by environment as follows: circles for isolated galaxies, asterisks for interacting/merging galaxies, filled triangles for Virgo galaxies, and squares for others.

simplest interpretation of the fact that the slope of the $L_{IR}-L(H\alpha)$ correlation is 1.0 argues that *the IR luminosity is a measure of the SFR for these galaxies*.

In Figure 6*b* we show the comparison of $L_{IR}/M(H_2)$ with the global equivalent width of Hα (EWHα) for the same galaxies. The EWHα measures the Hα flux normalized by the underlying red continuum and indicates the ratio of the present massive star formation rate to the star formation rate integrated over the lifetime of the galaxy. Thus, galaxies with a high EWHα are forming unusually large numbers of high-mass stars at the present time relative to star formation in the past.

We find a good correlation between the ratio $L_{IR}/M(H_2)$ and the EWHα for the 26 galaxies of type later than Sbc (correlation coefficient = 0.86; see Fig. 6*b*), such that

$$\mathrm{EWH}\alpha = 11\left[L_{IR}/M(H_2)\right]^{0.5}, \tag{13}$$

where EWHα is in A and $L_{IR}/M(H_2)$ is in units of $L_\odot/M_\odot$. This correlation suggests that *galaxies that are forming unusually large numbers of high-mass stars are doing so through efficient conversion of their gas reservoir to stars.* Given the dust temperature dependence of the $L_{IR}/M(H_2)$ ratio found in equation (11), the EWHα is also shown to have a dust temperature dependence. A straightforward interpretation of this result suggests that galaxies that have high Hα equivalent widths, and therefore high current massive star formation rates, have radiation fields with high energy densities which heat the dust to higher temperatures than in galaxies with lower massive star formation rates. The lower EWHα for the early-type galaxies was shown by Kennicutt and Kent (1983) to arise from the large contribution to the underlying red continuum by the numerous stars in the bulge.

The data in Figure 6*c* are coded by total luminosity ($L_{IR}+L_B$) for the 26 late-type galaxies. The galaxies with the lowest luminosities ($L<10^{10}$ $L_\odot$) and high values of $L_{IR}/M(H_2)$, although few in number, all have higher values of $L_{IR}/M(H_2)$ for their EWHα than the more luminous galaxies. This displacement for low-relative to high-luminosity galaxies may result from the higher H I/H_2 ratio in low-luminosity galaxies and the more significant contribution by dust in the H I clouds in these galaxies to the total IR luminosity.

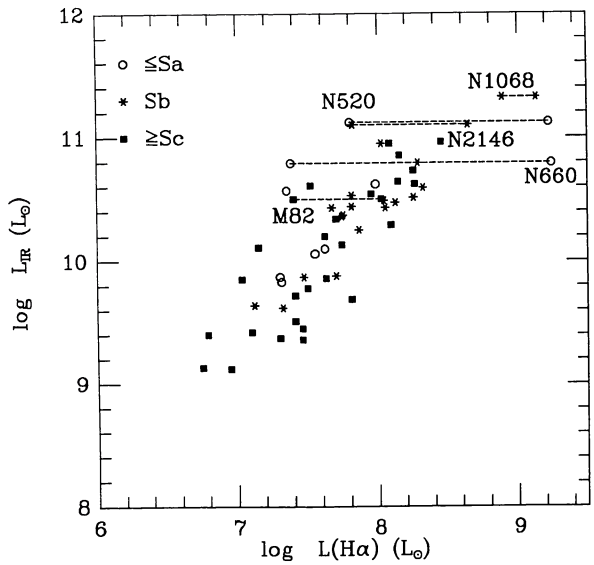

FIG. 6*a*

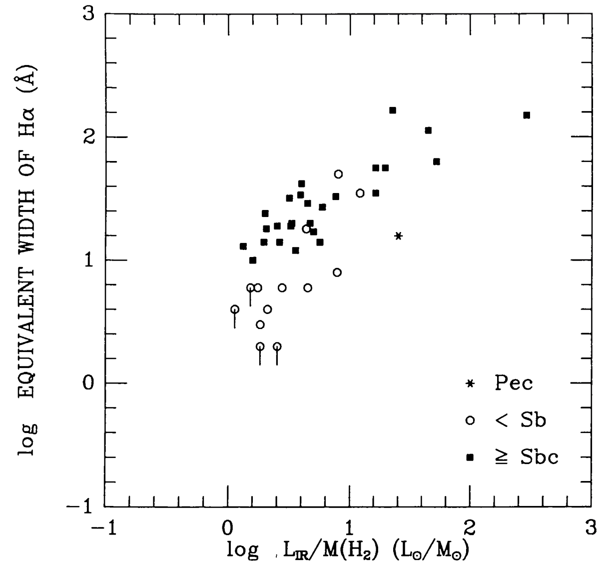

FIG. 6*b*

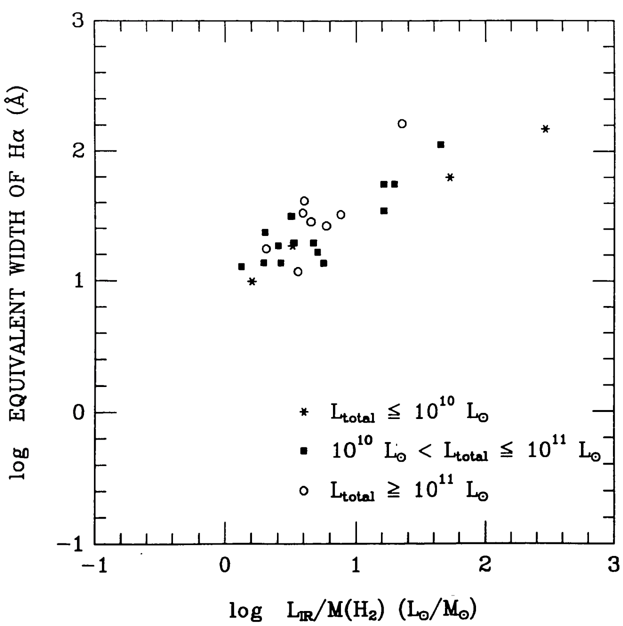

FIG. 6*c*

FIG. 6.—Comparison of IR and Hα luminosities. For the five galaxies in which extinction corrections have been made (Young, Kleinmann, and Allen 1988), both the observed and corrected Hα luminosities are indicated and connected by a dashed line. Points are coded by morphological type: circles for ≤ Sa, asterisks for Sb, and squares for Sc and others. (*b*) Comparison of the Hα equivalent width (EWHα) with $L_{IR}/M(H_2)$, where galaxy types are indicated as follows: circles for early types (≤ Sb), filled squares for late types (≥ Sbc), and asterisks for peculiars. The galaxies classified as type Sbc and later are shown in (*c*). (*c*) Comparison of the EWHα with $L_{IR}/M(H_2)$ for 26 galaxies of type Sbc and later. Points are coded by total luminosity ($L_{IR} + L_B$), with asterisks for $L_{total} < 10^{10} L_\odot$, squares for $L_{total} = 10^{10}$–10^{11} $L_\odot$, and circles for $L_{total} > 10^{11}$ $L_\odot$.

VI. CONCLUSIONS

From a study of the infrared emission in 182 galaxies, we find the following:

1. The PSC underestimates the IR emission for galaxies larger than 4′ across. Flux densities derived from one- and two-dimensional co-added *IRAS* Survey data recover the extended emission, but there are 10–15% differences in the calibration relative to the PSC. We have corrected for these systematic calibration differences in this work.

2. We find an excellent correlation between the mass of warm dust emitting at 60–100 μm and the H_2 mass. The mean value of the ratio $M(H_2)/M_{dust} = 570 \pm 50$ for this sample.

3. We find the slopes of the fits to the comparisons of L_{IR} with $M(H_2)$ and M(H I) to be 1.0 ± 0.03, while the slopes of the fits to the comparisons of L_B with $M(H_2)$ and M(H I) to be 0.7 ± 0.03. We suggest that extinction of the blue light in the luminous galaxies may cause the difference in the slopes, since the more luminous galaxies have higher H_2 and dust column densities in the inner disks. For the comparisons of atomic and molecular gas masses with IR and blue luminosities, the best correlations found are those involving H_2 masses.

4. We find a good correlation between L_{IR} and L(Hα) for 49 galaxies, supporting the suggestion that the IR luminosity measures the rate of star formation in these galaxies. It then follows that the ratio $L_{IR}/M(H_2)$ measures the rate of star formation per unit mass of H_2, which we call the efficiency of star formation.

5. We find similar ranges in the yield of young stars per unit mass of molecular gas, $L_{IR}/M(H_2)$ for early- and late-type spiral galaxies.

6. We find a good correlation between the Hα equivalent width and $L_{IR}/M(H_2)$ for 26 late-type spiral galaxies with L_{IR} from 10^9 and to 10^{12} $L_\odot$, and suggest that galaxies which are forming many massive stars are doing so through efficient conversion of their gas into stars.

Finally, we note that more observations of the Hα, H_2, H I, and cold dust content of galaxies are needed to address the questions raised in this study. Specifically, it will be necessary to know the spatial *distributions* of the dust, ionized gas, molecular gas, and atomic gas components in galaxies to enable a complete interpretation of the evolution of these systems.

It is a pleasure to thank the staff of IPAC for providing assistance during a number of visits to the facility; thanks also to C. Lonsdale for a careful reading of the manuscript. Support for this research was provided by NASA's *IRAS* Data Analysis Program and funded through the Jet Propulsion Laboratory.

REFERENCES

Becklin, E., and Wynn-Williams, G. 1987, in *Proceedings of Star Formation in Galaxies*, ed. C. Lonsdale (Washington, DC: NASA), p. 643.
Bloemen, J. B. G. L., *et al.* 1986, *Astr. Ap.*, **154**, 25.
Brinks, E. 1984, Ph.D. thesis, Sterrewacht Leiden.
Bushouse, H. 1986, Ph.D. thesis, University of Illinois.
Cataloged Galaxies and Quasars Observed in the IRAS Survey. 1985, prepared by C. J. Lonsdale, G. Helou, J. C. Good, and W. Rice (Washington, DC: Jet Propulsion Laboratory).
de Jong, T., *et al.* 1984, *Ap. J.* (*Letters*), **278**, L67.
De Gioia-Eastwood, K., Grasdalen, G. L., Strom, S. E., and Strom, K. M. 1984, *Ap. J.*, **278**, 564.
de Vaucouleurs, G., de Vaucouleurs, A., and Buta, R. 1981, *A.J.*, **86**, 1429.
de Vaucouleurs, G., de Vaucouleurs, A., and Corwin, H. G. 1976, *Second Reference Catalogue of Bright Galaxies* (Austin: University of Texas Press) (RC2).
Dickman, R. L., Snell, R. L., and Schloerb, F. P. 1986, *Ap. J.*, **309**, 326.
Draine, B. T., and Lee, H. M. 1984, *Ap. J.*, **285**, 89.
Dressel, L. L., and Condon, J. J. 1976, *Ap. J. Suppl.*, **31**, 187.
Gautier, T. N. 1986, in *Light On Dark Matter*, ed. F. P. Israel (Dordrecht: Reidel).
Giovanelli, R., and Haynes, M. P. 1985, *Ap. J.*, **292**, 404.
Harwit, M., Houck, J. R., Soifer, B. T., and Palumbo, G. G. C. 1986, preprint.
Hildebrand, R. H. 1983, *Quart. J.R.A.S.*, **24**, 267.
Huchra, J. 1985, private communication.
Huchtmeier, W. K., Richter, O.-G., Bohnenstengel, H.-D., and Hauschildt, M. 1983, *A General Catalog of H* I *Observations of External Galaxies*, ESO Prepreint No. 250.
IRAS Point Source Catalog. 1985, Joint *IRAS* Science Working Group (Washington, DC: GPO).
Iyengar, K. V. K., Rengarajan, T. N., and Verma, R. P. 1985, *Astr. Ap.*, **148**, 43.
Kenney, J. 1987, Ph.D. thesis, University of Massachusetts, Amherst.
Kenney, J., and Young, J. 1988*a*, *Ap. J.*, **326**, 588.
______. 1989, *Ap. J.*, submitted.
______. 1988*b*, *Ap. J. Suppl.*, **66**, 261.
Kennicutt, R. C., Jr., Keel, W., van der Hulst, J. M., Hummel, E., and Roettiger, K. A. 1987, *A.J.*, **93**, 1011.
Kennicutt, R. C., Jr. and Kent, S. M. 1983, *A.J.*, **88**, 1094.
Leggett, S. K., Brand, P. W. J. L., and Mountain, C. M. 1987, *M.N.R.A.S.*, in press.
Lonsdale, C., and Helou, G. 1987, *Ap. J.*, **314**, 513.
Lord, S., and Young, J. S. 1988, in preparation.
Low, F., *et al.* 1984, *Ap. J.* (*Letters*), **278**, L19.
Maloney, P. 1987, Ph.D. thesis, University of Arizona.
Morris, M., and Rickard, L. J. 1982, *Ann. Rev. Astr. Ap.*, **20**, 517.
Nilson, P. 1973, *Uppsala General Catalogue of Galaxies* (Uppsala: Uppsala Observatory) (UGC).
Pagel, B. E. J., and Edmunds, M. G. 1981, *Ann. Rev. Astr. Ap.*, **19**, 77.
Rengarajan, T. N., and Iyengar, K. V. K. 1988, *J. Ap. Astr.*, **9**, 79.
Rice, W. L., *et al.* 1988, *Ap. J. Suppl.*, in press.
Rieke, G. H., Lebofsky, M. J., Thompson, R., Low, F., and Tokunaga, A. 1980, *Ap. J.*, **238**, 24.
Roberts, M. S. 1969, *A.J.*, **74**, 859.
Rowan-Robinson, M., and Crawford, J. 1986, in *Light On Dark Matter*, ed. F. P. Israel (Dordrecht: Reidel).
Sanders, D. B., *et al.* 1986, *Ap. J.* (*Letters*), **305**, L45.
Scoville, N., Yun, M., Clemens, D., Sanders, D., Waller, W. 1987, *Ap. J.* (*Suppl*)., **63**, 821.
Scoville, N. Z., and Good, J. 1988, preprint.
Scoville, N. Z., and Sanders, D. B. 1987, in *Interstellar Processes*, ed. D. Hollenbach and H. Thronson (Dordrecht: Reidel), p. 21.
Scoville, N. Z., Soifer, B. T., Neugebauer, G., Young, J. S., Mathews, K., and Yerka, J. 1985, *Ap. J.*, **289**, 129.
Scoville, N. Z., and Young, J. S. 1983, *Ap. J.*, **265**, 148.
Scoville, N. Z., Young, J. S., and Lucy, L. 1983, *Ap. J.*, **270**, 443.
Searle, L., Sargent, W. L. W., and Bagnuolo, W. 1973, *Ap. J.*, **179**, 427.
Shostak, G. S. 1978, *Astr. Ap.*, **68**, 321.
Smith, J. 1982, *Ap. J.*, **261**, 463.
Smith, J., Harper, D. A., and Lowenstein, R. F. 1984, in *Airborne Astronomy Symposium*, ed. H. Thronson and X. Erickson, (Washington, DC: NASA), p. 277.
Soifer, B. T., *et al.* 1984, *Ap. J.* (*Letters*), **278**, L71.
Solomon, P. M., and Sage, L. 1988, *Ap. J.*, in press.
Stark, A. A. 1979, Ph.D. thesis, Princeton University.
Stark, A. A., Knapp, G. R., Bally, J., Wilson, R. W., Penzias, A. A., and Rowe, H. E. 1986, *Ap. J.*, **310**, 660.
Tacconi, L., and Young, J. S. 1986, *Ap. J.*, **308**, 600.
______. 1987, *Ap. J.*, **322**, 681.
Telesco, C. M., and Harper, D. A. 1980, *Ap. J.*, **235**, 392.
Tinsley, B. M. 1980, in *Fundamentals of Cosmic Physics*, Vol. **5** (London: Gordon and Breach), p. 287.
van Gorkom, J., and Kotanyi, K. 1985, in *ESO Workshop on the Virgo Cluster of Galaxies*, ed. O.-G. Richter and B. Bingelli, (Garching: ESO), p. 51.
Verter, F. 1987, *Ap. J. Suppl.*, **65**, 555.
Walterbos, R. M. 1987, in *Galactic and Extragalactic Star Formation*, ed. M. Fich and R. Pudritz (Dordrecht: Kluwer).
Warmels, R. H. 1986, Ph.D. thesis, Groningen.
Young, E. T., *et al.* 1985, *IPAC Rept. No. 1, A User's Guide to the IRAS Pointed Observation Products*, (Washington, DC: GPO).
Young, J. S., Kenney, J., Lord, S., and Schloerb, F. P. 1984, *Ap. J.* (*Letters*), **287**, L65.
Young, J. S., Kenney, J. D., Tacconi, L., Claussen, M. J., Huang, Y.-L., Tacconi-Garman, L., Xie, S., Schloerb, F. P. 1986*a*, *Ap. J.* (*Letters*), **311**, L17.
Young, J. S., Kleinmann, S. G., and Allen, L. 1988, *Ap. J.* (*Letters*), in press.
Young, J. S., *et al.* 1989, in preparation.
Young, J. S., Schloerb, F. P., Kenney, J., and Lord, S. 1986*b*, *Ap. J.*, **304**, 443.
Young, J. S., and Scoville, N. Z. 1982*a*, *Ap. J.*, **258**, 467.
______. 1982*b*, *Ap. J.* (*Letters*), **260**, L11.
______. 1982*c*, *Ap. J.* (*Letters*), **260**, L41.
______. 1984, *Ap. J.*, **287**, 153.
Young, J. S., Tacconi, L., and Scoville, N. 1983, *Ap. J.*, **269**, 136.

J. D. P. Kenney: Astronomy Department, Caltech, 105-24, Pasadena, CA 91125

W. L. Rice: IPAC, Pasadena, CA 91125

S. Xie and J. S. Young: Department of Physics and Astronomy and Five College Radio Astronomy Observatory, University of Massachusetts, Amherst, MA 01003